haematologica
Journal of the Ferrata Storti Foundation

Oncolytic bovine herpesvirus type 1 induces immune microenvironment remodeling and enhances treatment responses in multiple myeloma

by Vincenzo Raimondi, Rosanna Vescovini, Paola Storti, Valentina Franceschi, Giulia Pozzi, Camilla Sitzia, Nicolas Thomas Iannozzi, Denise Toscani, Benedetta Dalla Palma, Matteo Scita, Mattia Dessena, Sergio Minesso, Stefania Ricci, Fazel Mohammadi, Oxana Lungu, Prisco Mirandola, Gaetano Donofrio and Nicola Giuliani

Received: September 30, 2025.
Accepted: March 11, 2026.

Citation: Vincenzo Raimondi, Rosanna Vescovini, Paola Storti, Valentina Franceschi, Giulia Pozzi, Camilla Sitzia, Nicolas Thomas Iannozzi, Denise Toscani, Benedetta Dalla Palma, Matteo Scita, Mattia Dessena, Sergio Minesso, Stefania Ricci, Fazel Mohammadi, Oxana Lungu, Prisco Mirandola, Gaetano Donofrio and Nicola Giuliani. Oncolytic bovine herpesvirus type 1 induces immune microenvironment remodeling and enhances treatment responses in multiple myeloma. Haematologica. 2026 Mar 26. doi: 10.3324/haematol.2025.289317 [Epub ahead of print]

Oncolytic bovine herpesvirus type 1 induces immune microenvironment remodeling and enhances treatment responses in multiple myeloma

Vincenzo Raimondi[1], Rosanna Vescovini[1], Paola Storti[1], Valentina Franceschi[2], Giulia Pozzi[1], Camilla Sitzia[1], Nicolas Thomas Iannozzi[1], Denise Toscani[1,3], Benedetta Dalla Palma[3], Matteo Scita[3], Mattia Dessena[1], Sergio Minesso[2], Stefania Ricci[1], Fazel Mohammadi[1], Oxana Lungu[1], Prisco Mirandola[1], Gaetano Donofrio[2] and Nicola Giuliani[1,3]

[1]Department of Medicine and Surgery, University of Parma, Parma, Italy.

[2]Department of Medical-Veterinary Science, University of Parma, Parma, Italy.

[3]Hematology, "Azienda Ospedaliero-Universitaria di Parma", Parma, Italy.

Address Correspondence to:

Nicola Giuliani, MD, PhD
Department of Medicine and Surgery
University of Parma
Via Gramsci 14, 43126, Parma, Italy
Tel: +390521033299; email: nicola.giuliani@unipr.it

Gaetano Donofrio, DVM, PhD
Department of Medical Veterinary Science,
University of Parma
Via del Taglio 8, 43126, Parma, Italy
Tel: +390521033299; email: gaetano.donofrio@unipr.it

DECLARATIONS

Funding

This work was supported by a grant from "Bando di Ateneo per la Ricerca 2021 - Azione A" (MUR_DM737_A_MEDCHIR_GIULIANI).

Acknowledgements

We thank the Associazione Italiana contro Leucemie, Linfomi e Mielomi ONLUS and ParmAIL for their support.

Authors' contributions

VR performed all in vitro experiments, with support from RV, PS, VF, GP, CS, NTI, DT, MD, SM, and OL. The oncolytic virus was provided by VF, SM, and GD. Flow cytometry analysis was conducted by RV and VR. Clinical samples were provided by BDP and MS. SR was responsible for patient enrolment and clinical data management. Bioinformatic analysis was performed by VR and FM. Data analysis and manuscript writing were carried out by VR, RV, GD, and NG. PS, PM, GD, and NG contributed to the interpretation of the data. PM, GD, and NG provided critical revision and approved the final version of the manuscript. All authors read and approved the final manuscript.

Competing interests

NG received research funding and honoraria from Amgen, Bristol-Myers Squibb, Celgene, Pfizer, Takeda, Millennium Pharmaceutical, and Janssen Pharmaceutical.

The other authors declare no competing financial interests.

Availability of data and materials

All data generated or analyzed during this study are included in this published article and its supplementary information files.

ABSTRACT

Despite therapeutic advances, multiple myeloma (MM) remains incurable due to the development of drug resistance by malignant plasma cells (PCs) and a severe immunosuppressive bone marrow (BM) microenvironment. Oncolytic virotherapy offers the dual benefit of tumor cell lysis and immune activation, but the efficacy of human viruses is often hampered by pre-existing antiviral immunity. Here, we demonstrated that bovine herpesvirus type 1 (BoHV-1), a virus that is non-pathogenic to humans, efficiently infected MM cells, inducing mitochondrial apoptosis and suppressing pro-survival programs, including MYC targets, oxidative phosphorylation, and the unfolded protein response. Infected tumor cells upregulated NK-activating ligands and downregulated MHC class I, enhancing susceptibility to NK-mediated cytotoxicity. In patient-derived BM mononuclear cells (BMMCs), BoHV-1 selectively reduced malignant PCs and immunosuppressive myeloid subsets, while sparing lymphoid populations and hematopoietic progenitors. The infection promoted activation of $CD8^+$ T cells, NK cells, and monocytes, driving a shift toward a pro-inflammatory M1-like polarization. Monocyte depletion in BMMCs attenuated the BoHV-1 anti-MM effect, confirming their functional contribution. This pronounced immune remodeling was accompanied by an inflammatory cytokine storm dominated by type I/II interferons and key innate immune mediators. Co-treatment of BoHV-1 with either bortezomib or lenalidomide increased anti-MM cytotoxicity. Finally, BoHV-1 upregulated CD38 on both MM cells and immune effectors, thereby increasing sensitivity to the anti-CD38 daratumumab. These findings establish BoHV-1 as a promising immunovirotherapy agent, effective as a single agent and in combination strategies, by coupling direct oncolysis with broad immune remodeling of the BM microenvironment.

KEYWORDS

Bone Marrow Microenvironment; Multiple Myeloma; Cell Therapy and Immunotherapy; Combination Therapy; Oncolytic Virus

INTRODUCTION

Multiple myeloma (MM) is a clonal malignancy of plasma cells (PCs) originating within the bone marrow (BM), leading to several clinical complications.[1] Despite advancements in therapeutic approaches, MM remains an incurable disease, as patients experience multiple relapses and eventually develop resistance to conventional anti-MM therapies.[1,2]

Immune dysregulation is a feature of MM patients and is involved in the pathophysiology of the disease and therapeutic response.[3] Interactions between MM cells and immune cells within the BM microenvironment are associated with the formation of a milieu favorable to tumor survival and progression.[4] Notably, T cells display transcriptional signatures of exhaustion, whereas NK cells, monocytes, and macrophages exhibit functional impairments that facilitate immune evasion, underscoring the rationale for immunotherapy-based strategies in MM.[5-10]

Oncolytic viruses (OVs) are immunotherapeutic agents that couple selective tumor cell killing with the induction of systemic anti-tumor immunity.[11] Several human viruses have been explored as oncolytic vectors, with efforts focused on attenuating pathogenicity and enhancing immunogenicity.[12] In MM, measles virus (MV) and reovirus (RV) advanced to early-phase trials but showed limited efficacy: MV-based therapy amplified anti-MM T cell activity without inducing objective responses, while RV monotherapy achieved only transient disease stabilization.[13,14] More broadly, the therapeutic promise of human OVs is constrained by host immunity, as antiviral responses and pre-existing neutralizing antibodies often limit viral replication and persistence.[15] These challenges have fueled interest in non-human OVs, which circumvent pre-existing immunity. Preclinical studies have highlighted vesicular stomatitis virus (VSV) and bovine viral diarrhea virus (BVDV) as promising candidates.[16,17] However, early clinical testing of VSV in relapsed/refractory MM (RRMM) yielded only stable disease despite an acceptable safety profile.[16]

Collectively, these findings underscore the need for novel OVs with distinct biological properties and improved efficacy.[17]

Bovine herpesvirus type 1 (BoHV-1) is a double-stranded DNA virus belonging to the Alphaherpesvirinae subfamily and responsible for bovine respiratory disease.[18,19] Structurally, BoHV-1 closely resembles herpes simplex virus 1 and employs similar attachment and entry receptors, including heparan sulfate proteoglycans (HSPGs), the nectin-1 (CD111), and the poliovirus receptor (CD155).[20,21] Preclinical studies have shown that oncogenic KRAS signaling can enhance BoHV-1 replication in selected tumor models; however, viral replication is not strictly required for BoHV-1-mediated tumor cell killing.[22]

It is known that BoHV-1 does not productively infect normal human cells;[23,24] instead, it selectively targets immortalized, transformed, and breast cancer-initiating cells.[24,25] Moreover, in a melanoma mouse model, it has been demonstrated that virus replication is not required for oncolytic BoHV-1 immunotherapy effects, suggesting that its anti-tumor activity may be uncoupled from its ability to replicate and induce cytopathic effect.[26]

The oncolytic activity of BoHV-1 has never been explored in hematological malignancies, but its unique biological and immunological features support it as a promising candidate for oncolytic virotherapy in MM. Here we demonstrated that, besides a direct oncolytic effect, BoHV-1 provides a potent immunovirotherapy that, in combination with anti-MM therapies, may improve overall treatment outcomes.

METHODS

Cell lines and reagents

All bovine and human cell lines, along with their respective culture conditions, were maintained as described in the Supplementary Methods.

Ethics approval and consent to participate

Patient samples were obtained after informed consent in accordance with the Declaration of Helsinki. This study was approved by the Ethics Committee "Area Vasta Emilia Nord" of the Regional Health Service, Italy (protocol code: 69/2023/TESS/UNIPR; CE:21/03/2023).

Patient samples and cell isolation

A total cohort of 39 consecutive patients with MM was included in the study: 28 newly diagnosed MM (NDMM) (median age 68 years; range 46-94) and 11 RRMM (median age 74 years; range 58-83). All patients were diagnosed according to the International Myeloma Working Group (IMWG) revised criteria.[27] Cytogenetic risk was defined according to the IMS/IMWG 2024 consensus recommendations.[28] The main characteristics of all the patients enrolled in the study are summarized in Supplementary Table S1. Patients' BM mononuclear cells (BMMCs) were isolated by Ficoll density gradient centrifugation. $CD138^+$ PCs were purified by positive magnetic selection, and monocytes were depleted using anti-CD14 magnetic microbeads. Detailed protocols for cell isolation and culture conditions are provided in the Supplementary Methods.

Virus propagation, infection, and drug treatments

BoHV-1 wild-type (strain Cooper, ATCC) was propagated as previously described.[29] Human myeloma cell lines (HMCLs), HS-5 stromal cells, patient-derived $CD138^+$ PCs, and BMMCs were treated with BoHV-1 at 1 and 2 MOI. BMMCs were also treated with heat-inactivated BoHV-1 (2 MOI). Cell-free supernatants were collected from BMMC cultures for subsequent analyses. Combination treatments with bortezomib (BTZ), lenalidomide (LENA), daratumumab (DARA), and elranatamab (ELRA) were performed either concurrently with BoHV-1 infection or sequentially.

Detailed protocols for virus propagation, infection, and drug treatments are provided in the Supplementary Methods.

In vitro blockade of CD111, CD155, and CD138 receptors

Blocking experiments targeting CD111, CD155, and CD138 putative BoHV-1 receptors were performed as described in the Supplementary Methods.

NK cell-mediated cytotoxicity assay

NK-92-mediated cytotoxicity against BoHV-1-pretreated JJN-3 cells was evaluated by flow cytometry using calcein-AM staining, as detailed in the Supplementary Methods.

Cytokine detection by ELISA

Levels of IFN-α, TNF-α, IFN-γ, IL-6, and IL-1β in cell-free BMMCs supernatants were measured by ELISA, as detailed in the Supplementary Methods.

Flow cytometry

Immunophenotyping, viability, apoptosis, degranulation, and activation marker analyses were performed by multiparametric flow cytometry using standardized protocols and antibody panels, as detailed in the Supplementary Methods. Gating strategies and data analysis procedures are provided in Supplementary Figures S1 and S2.

Bulk RNA sequencing

Total RNA was extracted from untreated and BoHV-1-treated JJN-3 cells, and RNA-seq libraries were prepared and sequenced on an Illumina NovaSeq platform. Reads were processed, aligned to the human genome (GRCh38), and quantified using standard bioinformatics pipelines. Differential gene expression analysis was performed using DESeq2, and gene set enrichment analysis (GSEA) was conducted as detailed in the Supplementary Methods. Further methodological details, including software versions, quality control, and thresholds, are provided in the Supplementary Methods.

Immunoblot

Immunoblotting analyses were performed as described in the Supplementary Methods.

Statistical analysis

Data are presented as mean ± standard deviation (SD) for cell lines and as median with interquartile range (IQR) for primary cells. Parametric and non-parametric tests were applied as appropriate, including one-way ANOVA with Tukey's test and the Friedman test with Dunn's correction. Correlations were assessed by Spearman's method. All statistical tests were two-sided, with a significance threshold set at $p < 0.05$. Further details are provided in the Supplementary Methods.

RESULTS

BoHV-1 infection elicits intrinsic apoptosis and suppresses survival pathways in HMCLs

To investigate the susceptibility of malignant PCs to BoHV-1, we profiled the surface expression of canonical viral attachment and entry receptors, CD111 and CD155, across a panel of HMCLs. Given the role of HSPGs in viral attachment, we also assessed the expression of syndecan-1 (CD138), a predominant HSPG and well-known hallmark of PCs. Flow cytometry analysis revealed high, albeit heterogeneous, expression of CD111 and CD155 across JJN-3, MM1.S, and OPM-2 cells, accompanied by uniformly elevated CD138 levels, as expected, delineating a receptor landscape compatible with BoHV-1 entry (Figure 1A).

To functionally evaluate BoHV-1 treatment, the HMCLs were infected at 1 and 2 MOI, and cell mortality was monitored via 7-AAD staining. All HMCLs, including OPM-2 cells (KRAS wild-type), displayed a progressive, MOI- and time-dependent increase in cell death, with significant cytotoxicity at 48 h and further exacerbation at 72 h post-infection (Figure 1B), consistent with a robust cytopathic effect.

To confirm the involvement of BoHV-1 attachment and entry receptors, MM1.S cells were pre-incubated with blocking antibodies targeting CD111, CD155, and CD138 antigens. The dual blockade of CD111 and CD155 significantly reduced BoHV-1-induced cytotoxicity, and this effect was further enhanced by concurrent blockade of CD138 (Supplementary Figure S3A), suggesting that BoHV-1 entry is at least partially dependent on the coordinated expression of these surface receptors.

Next, we assessed whether BoHV-1-induced cytotoxicity was mediated by apoptosis. Flow cytometric analysis revealed a time-dependent increase in apoptotic cells at 48 h and 72 h post-infection (Figure 2A), corroborated by immunoblot detection of cleaved pro-caspase-3 at 48 h (Figure 2B), indicating activation of the intrinsic apoptotic cascade.

To investigate the broader transcriptional response to BoHV-1, we performed bulk RNA sequencing of JJN-3 cells infected at 1 MOI for 24 h. Differential expression analysis identified 1,075 upregulated and 216 downregulated transcripts (FDR < 0.0005; Figure 2C). GSEA using the MSigDB Hallmark gene sets revealed significant enrichment of apoptosis, p53 signaling, TNFα signaling via NF-κB, and inflammatory response (Figure 2D), aligning with phenotypic evidence of cell death and inflammatory activation.

Conversely, gene sets related to proliferation and metabolic fitness were significantly downregulated, including MYC targets, oxidative phosphorylation, and the unfolded protein response (UPR), a pathway critical for proteostasis in immunoglobulin-producing cells (Figure 2D). KEGG pathway analysis supported these findings, highlighting extensive transcriptional remodeling during BoHV-1 infection (Supplementary Figure S3B).

BoHV-1 targets malignant PCs in the primary BM microenvironment

To validate our HMCLs' findings on the primary BM setting, we evaluated the expression of BoHV-1 attachment and entry receptors in BMMCs from MM patients. Representative flow cytometry

histograms of CD111, CD155, and CD138 expression in the major immune cell subsets from one patient are displayed in Supplementary Figure S4A. Cohort-wide analysis confirmed that CD111 and CD155 were most abundantly expressed on myeloid cells (both non-monocyte myeloid cells and monocytes), followed by PCs and hematopoietic stem and progenitor cells (HSPCs), with no detectable expression in T cells, NK cells, and B cells (Figure 3A). As expected, the expression of CD138 was consistently restricted to the PC compartment (Figure 3A). Given that stromal cells provide the structural backbone of hematopoietic and PC niches,[30] yet are challenging to identify within BMMCs, we employed the stromal cell line HS-5 to assess the expression of BoHV-1 attachment and entry receptors in non-hematopoietic cells. Flow cytometric analysis revealed minimal surface expression of CD111 and CD155 (Supplementary Figure S4B), suggesting a restricted capacity for viral infection.

To assess the susceptibility of primary PCs to BoHV-1 infection, the $CD138^+$ cells purified from patient-derived BMMCs were infected. A time- and dose-dependent significant reduction in viability was observed at 72 h and 96 h post-infection (Figure 3B), consistent with a direct cytopathic effect of the virus on MM PCs. Subsequently, we investigated the effect of BoHV-1 on total BMMCs from MM patients at 48 h, 72 h, and 96 h post-infection. As shown in a representative case (Supplementary Figure S4C), BoHV-1 treatment induced a progressive reduction in the percentage of MM PCs. Across the cohort, a significant time- and dose-dependent decrease in $CD138^+CD38^+$ cell viability was observed compared to untreated samples, with median viabilities of 79% and 73% at 48 h, 59% and 48% at 72 h, and 52% and 35% at 96 h for 1 and 2 MOI, respectively (Figure 3C). Treatment with heat-inactivated BoHV-1 did not affect PC viability in BMMCs, indicating that cytotoxicity requires intact viral structural proteins (Supplementary Figure S4D).

To determine whether the efficiency of BoHV-1-induced cytotoxicity correlated with tumor burden, we analyzed the association between baseline MM PC percentage in untreated BMMCs and post-infection viability. No significant correlation was observed (r = -0.1532; Figure 4A), suggesting that viral activity is independent of initial PC load. Furthermore, the extent of BoHV-1-mediated reduction in BM PC viability was comparable between NDMM and RRMM patients (Figure 4B) and across standard-risk (SR) and high-risk (HR) cytogenetic groups (Figure 4C).

To further characterize the impact of BoHV-1 beyond the malignant compartment, we analyzed its effect on non-tumor populations within the BMMCs. 96 h post-infection, BoHV-1 treatment resulted in a significant reduction of the percentage of myeloid cells, which was coupled to a significant increase of T, NK, and B percentages (Figure 4D). Notably, the percentage of HSPCs remained unchanged (Figure 4D). In line with receptor expression data, BoHV-1 exposure did not affect the viability of HS-5 stromal cells (Supplementary Figure S4E), indicating that the non-hematopoietic stromal population is not susceptible to virus-induced cytotoxicity.

BoHV-1 induces activation and cytotoxicity of immune effector cells and promotes immunogenic reprogramming of MM cells

It is well established that OVs exert anti-tumor effects both through direct oncolysis and by activating anti-tumor immune responses. Based on this, we investigated how BoHV-1 impacts effector cells within the BM microenvironment of MM patients.

In $CD8^+$ T cells, BoHV-1 treatment led to a significant upregulation of the early activation marker CD69 (Figure 5A) and CD107a (Figure 5B), a degranulation marker associated with cytolytic function. These findings are consistent with an initial functional priming of $CD8^+$ T cells upon viral exposure, observed at early time points.

NK cells displayed a similarly enhanced activation profile, with a robust increase in expression of CD69 (Figure 5C), CD38 (Figure 5D), and CD107a (Figure 5E), indicative of heightened metabolic

activity and cytotoxic function. This increase in CD38 expression progressed over 48 h, 72 h, and 96 h post BoHV-1 exposure (Supplementary Figure S5A), in parallel with the time-dependent reduction in PC viability.

We next examined whether BM NK cell activation correlated with immune-related transcriptional changes in tumor cells by interrogating the KEGG "Natural killer cell-mediated cytotoxicity" pathway within the BoHV-1 RNA-seq dataset from JJN-3 cells. This analysis revealed coordinated upregulation of multiple core constituent genes, including NK-activating ligands (MICA, MICB, ULBP3), alongside downregulation of classical HLA class I molecules (HLA-A, -B, -C), which normally suppress NK cell responses, as shown in Figure 5F.

To functionally validate this transcriptional signature, BoHV-1-pretreated JJN-3 cells were co-cultured with NK-92 cells for 4 h at increasing effector-to-target (E:T) ratios. Compared to untreated, virus-exposed targets exhibited significantly increased susceptibility to NK cell-mediated cytolysis (Figure 5G), confirming that BoHV-1 enhances NK recognition and cytotoxicity against MM cells.

BoHV-1 reshapes the myeloid BM landscape and drives anti-tumor immune activation

Based on our observation that BoHV-1 treatment reduces myeloid cells (Figure 4D), we further examined the virus's impact on specific myeloid subsets within the non-tumor BM compartment. First, $SSC^{high}CD11b^{+}$ cells were stratified into $CD14^{-}$ and $CD14^{dim/+}$ populations, corresponding to non-monocytic myeloid cells and mono/macrophages, respectively. At the later experimental time point, BoHV-1 treatment resulted in a significant reduction of $CD11b^{+}CD14^{-}$ cells, accompanied by a significant expansion of the $CD11b^{+}CD14^{dim/+}$ cells (Figure 6A). Then, within the $CD11b^{+}CD14^{-}$ subset, we considered the expression of CD16 to distinguish immature ($CD16^{-}$) from more mature myeloid cells ($CD16^{+}$). A significant reduction of $CD16^{+}$ cells was observed, paralleled by an increase in $CD16^{-}$ cells (Figure 6B), indicating a virus-driven reshaping of the non-monocytic

myeloid landscape with a predominant reduction in mature myeloid cells. Next, we investigated how BoHV-1 treatment impacts mono/macrophages. Specifically, exposure to BoHV-1 induced a significant and dose-dependent upregulation of both activation markers CD69 (Figure 6C) and CD38 (Figure 6D), detectable at 48 h and maintained through 96 h (Supplementary Figure S5B). Moreover, after 48 h of virus treatment, the percentage of $CD14^{+}CD16^{-}$ classical monocytes, typically associated with an M1-like anti-tumoral phenotype, increased significantly. In contrast, the rate of $CD14^{+}CD16^{+}$ non-classical monocytes, linked to an M2-like pro-tumoral phenotype, was significantly reduced (Figure 6E). This redistribution suggests that BoHV-1 actively drives mono/macrophage polarization toward an anti-tumor M1-like state.

To confirm the contribution of $CD14^{+}$ monocytes to the anti-MM activity of BoHV-1, we compared virus-treated total BMMCs with their CD14-depleted counterparts. Depletion of monocytes led to a significant increase in the viability of malignant PCs (Figure 6F), indicating that $CD14^{+}$ cells actively contribute to the virus's indirect oncolytic effects. Finally, we investigated the BM cytokine milieu in relation to BoHV-1 treatment. ELISA analysis revealed a significant increase in IFN-α, TNF-α, and IFN-γ levels in the supernatants of BoHV-1-treated compared to untreated BMMCs at 48 h post-infection (Figure 6G). At the later experimental time point, IL-6 and IL-1β levels were also significantly upregulated (Supplementary Figure S5C), consistent with a sustained inflammatory environment accompanying BoHV-1-mediated PC cytotoxicity.

BoHV-1 enhances the efficacy of clinically relevant anti-MM therapies

The limited efficacy of OVs as monotherapies, together with the reliance on combination regimens in MM, prompted us to test whether BoHV-1 could enhance the efficacy of clinically relevant anti-MM treatments.

Building on our transcriptomic analyses, which showed that BoHV-1 suppresses multiple proteostasis-related pathways, including the Hallmark UPR gene set (Figure 2D) and KEGG

Proteasome and Ribosome pathways (Supplementary Figure S3B), we tested its combination with BTZ, a proteasome inhibitor that induces proteotoxic stress. In preliminary experiments using the JJN-3 cell line, co-treatment with BoHV-1 (1 MOI) and BTZ (2, 3, 5 nM) significantly reduced cell viability compared to either agent alone (Supplementary Figure S6A). In MM patient-derived BMMCs (n=11), BoHV-1 (1 and 2 MOI) combined with BTZ (2 nM) significantly decreased PC viability (Figure 7A).

We further evaluated BoHV-1 in combination with the immunomodulatory drug LENA, chosen for its ability to enhance immune effector functions. In JJN-3 cells, co-treatment with BoHV-1 (1 MOI) and LENA (1, 2, 10 µM) reduced cell viability compared to either agent alone (Supplementary Figure S6B). A similar effect was observed in BMMCs from MM patients (n=9), where BoHV-1 combined with LENA (10 µM) significantly decreased PC viability (Figure 7B).

We then focused on the effects of BoHV-1 on CD38 expression, which was significantly upregulated not only on NK cells (Figure 5D) and monocytes (Figure 6D), but also on malignant PCs (Figure 7C). CD38 is a clinically relevant target of anti-MM monoclonal antibodies, including DARA. Accordingly, DARA (10 µg/mL) was administered 48 h post-infection (Figure 7D), corresponding to the time point at which CD38 upregulation was consistently observed in BM PCs. In patient-derived BMMCs (n=12), co-treatment with BoHV-1 and DARA significantly reduced PC viability (Figure 7E).

Finally, to explore BoHV-1 interactions with other immune-engaging agents, we assessed its combination with the bispecific antibody ELRA (BCMA×CD3). In BMMCs from MM patients (n=8), BoHV-1 (1 and 2 MOI) combined with a suboptimal dose of ELRA (0.01 nM), administered 24 h post-infection (Supplementary Figure S6C), significantly reduced PC viability (Supplementary Figure S6D).

DISCUSSION

The clinical efficacy of OVs in MM has remained modest, largely due to inefficient tropism for malignant PCs or pre-existing antiviral immunity that limits viral propagation.[13,14,16,17]

To overcome these barriers, non-human OVs represent a promising alternative. We previously showed that BVDV exerts direct cytotoxic effects on MM cells in both *ex vivo* and *in vivo* models.[31] Here, we extend this approach by investigating BoHV-1 as a novel oncolytic agent in MM, providing the first evidence that a bovine virus can reprogram the BM microenvironment from a "cold" immunosuppressive state into a "hot" pro-inflammatory and immunostimulatory niche.

Across MM cell lines, putative BoHV-1 attachment and entry receptors were consistently expressed at high levels, supporting a receptor landscape compatible with viral entry. Functionally, BoHV-1 infection induced marked cytopathic effects in all tested HMCLs, including the KRAS wild-type OPM-2 cells, accompanied by activation of the intrinsic apoptotic cascade.

Antibody-mediated blockade implicated CD138 in viral tropism, reinforcing the rationale for BoHV-1 targeting within the MM niche, although incomplete protection suggests involvement of additional host factors. Transcriptomic profiling further showed that BoHV-1 reprograms MM cells by inducing apoptotic, p53, and inflammatory pathways while suppressing MYC, oxidative phosphorylation, and UPR programs, thereby exploiting their dependence on proteostasis and mitochondrial metabolism.

In patient-derived BM samples, BoHV-1 attachment and entry receptors were highly expressed on PCs, monocytes, and non-monocyte myeloid cells, supporting the capacity to infect multiple cellular populations within the BM niche. Consistent with this distribution, BoHV-1 reduced PC viability and led to a decrease of myeloid cells with a relative increase in lymphoid subsets; this shift is more likely attributable to a selective decrease of myeloid cells rather than active

expansion of lymphoid subsets. Importantly, HSPCs remained unaffected by BoHV-1 treatment, underscoring the virus's selective cytotoxicity and its ability to preserve hematopoietic integrity.

Beyond its direct oncolytic activity, BoHV-1 infection markedly reshapes the immune microenvironment. $CD8^+$ T cells showed early functional priming upon viral exposure, whereas NK cells underwent a more pronounced activation, consistent with their intrinsic capacity for rapid innate responses. Infected MM cells upregulated NK-activating ligands while concomitantly downregulating classical HLA class I molecules, generating a surface phenotype that aligns with the observed increase in NK cell-mediated cytotoxicity and innate immune recognition.

It is well recognized that successful anti-MM immunotherapeutic strategies should overcome immunosuppressive barriers and redress the balance between immunogenic and tolerogenic inflammation in the BM microenvironment.[32,33] Analyzing the reduction of myeloid cells, we found that BoHV-1 infection led to a profound quantitative and qualitative remodeling of the myeloid compartment. The activation of mono/macrophages indicates their engagement in response to viral pattern recognition, while the significant skewing toward the $CD14^{dim/+}CD16^-$ subset reveals the virus-driven polarization from an M2-like pro-tumoral to a pro-inflammatory and anti-tumor M1-like phenotype. Interestingly, a previous study has reported a significantly higher enrichment of M2 tolerogenic macrophages in rapid progressors, supporting that virus-induced macrophage reprogramming may contribute to counteracting the immunosuppressive microenvironment associated with disease progression.[34] As expected, the result that the depletion of $CD14^+$ monocytes markedly reduced BoHV-1's ability to diminish PC viability confirms that these cells actively contribute to the virus's anti-tumor effects. At later experimental time points, among BoHV-1-treated BMMCs, we observed that the decrease in myeloid cells was associated with a change in their relative subset composition. Indeed, BoHV-1 treatment resulted in a significant

reduction of the non-monocyte myeloid cells, particularly those with a $CD16^+$ phenotype, counteracted by the increase in mono/macrophage frequency. We are unable to accurately identify myeloid-derived suppressor cells (MDSCs), but literature evidence suggests that cells with suppressive activity may be included among the more mature depleted $CD11b^+CD14^-CD16^+$ subset.[35,36] Of note, since viability analyses are based on relative frequencies within total BMMCs, the reduction of myeloid populations may partially mask the extent of PC loss and even underestimate BoHV-1's anti-tumor effect.

Consistent with a virus-driven shift toward an immunostimulatory BM environment, BoHV-1 exposure induced early increases in IFN-α, TNF-α, and IFN-γ that coincided with the onset of PC cytotoxicity. The increased levels of IL-6 and IL-1β observed at later time points may indicate that this inflammatory milieu persists beyond the initial cytotoxic phase. Although the absence of comprehensive kinetic profiling precludes formal causal inference, these data support a model in which BoHV-1 triggers a temporally evolving inflammatory program that accompanies, and may contribute to, its anti-MM activity.

Overall, these findings support a model in which direct BoHV-1-mediated oncolysis and concomitant immune remodeling within the BM microenvironment co-evolve and reinforce the anti-MM response, rather than acting as independent or strictly sequential processes.

Current MM treatment relies on multidrug regimens, typically including dexamethasone, immunomodulatory agents, proteasome inhibitors, and monoclonal antibodies targeting PC-associated antigens. Building on this rationale and the multifaceted activity of BoHV-1, we investigated its potential in combination with established anti-MM agents.

Transcriptomic analyses revealed downregulation of UPR and proteasome pathways, two critical stress-adaptation programs in MM, prompting the hypothesis that BoHV-1 might potentiate the effects of proteasome inhibition. Indeed, co-treatment with BTZ led to markedly enhanced cytotoxicity in a representative MM cell line and, most importantly, in primary patient samples. Beyond proteostasis collapse, BTZ is a well-characterized inducer of apoptosis through activation of caspase-8 and caspase-9 cascades converging on caspase-3,[37] whereas our functional studies demonstrated that BoHV-1 infection directly promotes mitochondrial apoptosis. Thus, the combination likely amplifies caspase-3-dependent cell death through complementary mechanisms. This effect may also extend to immunogenic cell death (ICD): proteasome inhibitors are recognized inducers of ICD, and a recent study has demonstrated that BoHV-1 alone can elicit bona fide ICD in immunocompetent tumor models.[38] Although we did not directly assess ICD in this setting, the observed immune activation and transcriptional remodeling are consistent with engagement of ICD pathways in MM.

Similarly, BoHV-1 treatment with LENA increased anti-tumor cytotoxicity across our experiments. This result may be due to the combination of both virus and drug direct antiproliferative effects on MM cells, as well as to shared pleiotropic effects on immune cells.[39] LENA promotes NK cell-mediated killing by inducing IKZF1/3 degradation and upregulating activating ligands.[40] BoHV-1 infection triggered comparable changes and increased NK activation, suggesting that the combination improves NK cell recognition and elimination of infected MM cells. In addition, LENA has been shown to repolarize MM-associated macrophages from an M2 to M1 phenotype and to enhance phagocytic activity in mouse models,[41,42] consistent with the immunostimulatory effects observed following BoHV-1 treatment alone.

To assess the translational relevance of BoHV-1 in contemporary MM immunotherapy, we examined its compatibility with antibody-based therapies. The virus-induced upregulation of CD38 on MM PCs, NK cells, and monocytes provides a strong biological rationale for combining with DARA. Increased CD38 expression may potentiate DARA-mediated cytotoxicity by enhancing target antigen density on tumor cells and facilitating Fc-dependent engagement of immune effector cells.[43] Consistent with this rationale, the results of a greater reduction in MM PC viability with co-treatment with DARA compared to either agent alone support the capacity of BoHV-1 to sensitize both tumor and immune effector compartments to anti-CD38 antibody-based therapies. In a more exploratory setting, administration of the BCMA×CD3 bispecific antibody ELRA after viral infection was associated with improved anti-MM activity, consistent with the hypothesis that BoHV-1-mediated immune remodeling may also favor T cell-redirecting approaches.[35,44]

A limitation of this study is the absence of *in vivo* preclinical validation. However, BoHV-1 does not efficiently bind to or enter murine cells, precluding the use of conventional mouse models and preventing faithful reproduction of virus-tumor-immune interactions.[23,45] Although pseudotyping with heterologous glycoproteins can enhance entry into murine cells, viral gene transcription remains inefficient due to intrinsic host defenses, and such approaches rely on engineered viruses not intended for clinical translation. Alternative species, such as cotton rats, have been used in anti-BoHV-1 vaccination studies and selected tumor models, but these systems are not established for MM.[46] In this context, patient-derived *ex vivo* BM cultures provide a biologically relevant human platform to assess BoHV-1 activity and combinatorial strategies within a complex and immunologically intact microenvironment. Future work may extend these findings using advanced human-based systems, including three-dimensional BM organoids or other *ex vivo* platforms that more faithfully recapitulate tissue architecture and long-term immune-tumor dynamics.

Ultimately, BoHV-1 lacks pre-existing human immunity, exerts potent therapeutic activity at low MOIs, requires no engineering, allows straightforward genetic manipulation,[47] and can be produced at scale on established platforms, making it a practical and versatile oncolytic candidate.

CONCLUSIONS

In conclusion, this study establishes BoHV-1 as a novel oncolytic agent capable of inducing direct cytotoxicity and deep immunologic remodeling in MM. These findings provide a strong rationale for further preclinical development of BoHV-1-based immunovirotherapy, potentially in combination with standard-of-care agents, to improve outcomes for MM patients.

REFERENCES

1. Malard F, Neri P, Bahlis NJ, et al. Multiple myeloma. Nat Rev Dis Primers. 2024;10(1):45.
2. Binder M, Nandakumar B, Rajkumar SV, et al. Mortality trends in multiple myeloma after the introduction of novel therapies in the United States. Leukemia. 2022;36(3):801-808.
3. Nakamura K, Smyth MJ, Martinet L. Cancer immunoediting and immune dysregulation in multiple myeloma. Blood. 2020;136(24):2731-2740.
4. Bailur JK, McCachren SS, Doxie DB, et al. Early alterations in stem-like/resident T cells, innate and myeloid cells in the bone marrow in preneoplastic gammopathy. JCI Insight. 2019;5(11):127807.
5. Zelle-Rieser C, Thangavadivel S, Biedermann R, et al. T cells in multiple myeloma display features of exhaustion and senescence at the tumor site. J Hematol Oncol. 2016;9(1):116.
6. Tirier SM, Mallm JP, Steiger S, et al. Subclone-specific microenvironmental impact and drug response in refractory multiple myeloma revealed by single-cell transcriptomics. Nat Commun. 2021;12(1):6960.
7. Noonan K, Borrello I. The immune microenvironment of myeloma. Cancer Microenviron. 2011;4(3):313-323.
8. von Lilienfeld-Toal M, Frank S, Leyendecker C, et al. Reduced immune effector cell NKG2D expression and increased levels of soluble NKG2D ligands in multiple myeloma may not be causally linked. Cancer Immunol Immunother. 2010;59(6):829-839.
9. Sun J, Park C, Guenthner N, et al. Tumor-associated macrophages in multiple myeloma: advances in biology and therapy. J Immunother Cancer. 2022;10(4):e003975.
10. Shah UA, Mailankody S. Emerging immunotherapies in multiple myeloma. BMJ. 2020;370:m3176.
11. Kaufman HL, Kohlhapp FJ, Zloza A. Oncolytic viruses: a new class of immunotherapy drugs. Nat Rev Drug Discov. 2015;14(9):642-662.
12. Lin D, Shen Y, Liang T. Oncolytic virotherapy: basic principles, recent advances and future directions. Signal Transduct Target Ther. 2023;8(1):156.
13. Packiriswamy N, Upreti D, Zhou Y, et al. Oncolytic measles virus therapy enhances tumor antigen-specific T-cell responses in patients with multiple myeloma. Leukemia. 2020;34(12):3310-3322.
14. Sborov DW, Nuovo GJ, Stiff A, et al. A phase I trial of single-agent reolysin in patients with relapsed multiple myeloma. Clin Cancer Res. 2014;20(23):5946-5955.
15. Gujar S, Pol JG, Kim Y, Lee PW, Kroemer G. Antitumor Benefits of Antiviral Immunity: An Underappreciated Aspect of Oncolytic Virotherapies. Trends Immunol. 2018;39(3):209-221.
16. Cook J, Peng KW, Witzig TE, et al. Clinical activity of single-dose systemic oncolytic VSV virotherapy in patients with relapsed refractory T-cell lymphoma. Blood Adv. 2022;6(11):3268-3279.
17. Raimondi V, Vescovini R, Dessena M, Donofrio G, Storti P, Giuliani N. Oncolytic viruses: a potential breakthrough immunotherapy for multiple myeloma patients. Front Immunol. 2024;15:1483806.
18. Zhang S, Wood C, Xue W, Krukenberg SM, Chen Q, Minocha HC. Immune suppression in calves with bovine immunodeficiency virus. Clin Diagn Lab Immunol. 1997;4(2):232-235.
19. Nataraj C, Eidmann S, Hariharan MJ, Sur JH, Perry GA, Srikumaran S. Bovine herpesvirus 1 downregulates the expression of bovine MHC class I molecules. Viral Immunol. 1997;10(1):21-34.
20. Campadelli-Fiume G, Cocchi F, Menotti L, Lopez M. The novel receptors that mediate the entry of herpes simplex viruses and animal alphaherpesviruses into cells. Rev Med Virol. 2000;10(5):305-319.

21. Tan WS, Rong E, Dry I, et al. Validation of Candidate Host Cell Entry Factors for Bovine Herpes Virus Type-1 Based on a Genome-Wide CRISPR Knockout Screen. Viruses. 2024;16(2):297.
22. Cuddington BP, Mossman KL. Permissiveness of human cancer cells to oncolytic bovine herpesvirus 1 is mediated in part by KRAS activity. J Virol. 2014;88(12):6885-6895.
23. Hushur O, Takashima Y, Matsumoto Y, Otsuka H. Restriction of bovine herpesvirus 1 (BHV-1) growth in non-permissive cells beyond the expression of immediate early genes. J Vet Med Sci. 2004;66(4):453-455.
24. Rodrigues R, Cuddington B, Mossman K. Bovine herpesvirus type 1 as a novel oncolytic virus. Cancer Gene Ther. 2010;17(5):344-355.
25. Cuddington BP, Dyer AL, Workenhe ST, Mossman KL. Oncolytic bovine herpesvirus type 1 infects and kills breast tumor cells and breast cancer-initiating cells irrespective of tumor subtype. Cancer Gene Ther. 2013;20(5):282-289.
26. Baracuhy EM, Cormier O, Davola ME, Collins S, Mossman K. Virus replication is not required for oncolytic bovine herpesvirus-1 immunotherapy. Mol Ther Oncol. 2024;32(4):200906.
27. Rajkumar SV. Multiple myeloma: 2024 update on diagnosis, risk-stratification, and management. Am J Hematol. 2024;99(9):1802-1824.
28. Avet-Loiseau H, Davies FE, Samur MK, et al. International Myeloma Society/International Myeloma Working Group Consensus Recommendations on the Definition of High-Risk Multiple Myeloma. J Clin Oncol. 2025;43(24):2739-2751.
29. Donofrio G, Franceschi V, Capocefalo A, et al. Cellular targeting of engineered heterologous antigens is a determinant factor for bovine herpesvirus 4-based vaccine vector development. Clin Vaccine Immunol. 2009;16(11):1675-1686.
30. de Jong MME, Chen L, Raaijmakers M, Cupedo T. Bone marrow inflammation in haematological malignancies. Nat Rev Immunol. 2024;24(8):543-558.
31. Marchica V, Franceschi V, Vescovini R, et al. Bovine pestivirus is a new alternative virus for multiple myeloma oncolytic virotherapy. J Hematol Oncol. 2020;13(1):89.
32. Malek E, de Lima M, Letterio JJ, et al. Myeloid-derived suppressor cells: The green light for myeloma immune escape. Blood Rev. 2016;30(5):341-348.
33. Asimakopoulos F, Hope C, Johnson MG, Pagenkopf A, Gromek K, Nagel B. Extracellular matrix and the myeloid-in-myeloma compartment: balancing tolerogenic and immunogenic inflammation in the myeloma niche. J Leukoc Biol. 2017;102(2):265-275.
34. Pilcher W, Thomas BE, Bhasin SS, et al. Cross center single-cell RNA sequencing study of the immune microenvironment in rapid progressing multiple myeloma. NPJ Genom Med. 2023;8(1):3.
35. Perez C, Botta C, Zabaleta A, et al. Immunogenomic identification and characterization of granulocytic myeloid-derived suppressor cells in multiple myeloma. Blood. 2020;136(2):199-209.
36. Veglia F, Sanseviero E, Gabrilovich DI. Myeloid-derived suppressor cells in the era of increasing myeloid cell diversity. Nat Rev Immunol. 2021;21(8):485-498.
37. Sogbein O, Paul P, Umar M, Chaari A, Batuman V, Upadhyay R. Bortezomib in cancer therapy: Mechanisms, side effects, and future proteasome inhibitors. Life Sci. 2024;358:123125.
38. Davola ME, Cormier O, Vito A, et al. Oncolytic BHV-1 Is Sufficient to Induce Immunogenic Cell Death and Synergizes with Low-Dose Chemotherapy to Dampen Immunosuppressive T Regulatory Cells. Cancers (Basel). 2023;15(4):1295.
39. Fink EC, Ebert BL. The novel mechanism of lenalidomide activity. Blood. 2015;126(21):2366-2369.
40. Fionda C, Abruzzese MP, Zingoni A, et al. The IMiDs targets IKZF-1/3 and IRF4 as novel negative regulators of NK cell-activating ligands expression in multiple myeloma. Oncotarget. 2015;6(27):23609-23630.

41. Mougiakakos D, Bach C, Bottcher M, et al. The IKZF1-IRF4/IRF5 Axis Controls Polarization of Myeloma-Associated Macrophages. Cancer Immunol Res. 2021;9(3):265-278.
42. Guo H, Yang J, Wang H, Liu X, Liu Y, Zhou K. Reshaping the tumor microenvironment: The versatility of immunomodulatory drugs in B-cell neoplasms. Front Immunol. 2022;13:1017990.
43. Horenstein AL, Faini AC, Morandi F, et al. Monoclonal anti-CD38 therapy in human myeloma: retrospects and prospects. Front Immunol. 2025;16:1519300.
44. van de Donk N, Chari A, Mateos MV. Mechanisms of resistance against T-cell engaging bispecific antibodies in multiple myeloma: implications for novel treatment strategies. Lancet Haematol. 2024;11(9):e693-e707.
45. Cuddington BP, Mossman KL. Oncolytic bovine herpesvirus type 1 as a broad spectrum cancer therapeutic. Curr Opin Virol. 2015;13:11-16.
46. Toth K, Spencer JF, Wold WS. Immunocompetent, semi-permissive cotton rat tumor model for the evaluation of oncolytic adenoviruses. Methods Mol Med. 2007;130:157-168.
47. Haque M, Stanfield B, Kousoulas KG. Bovine herpesvirus type-1 glycoprotein K (gK) interacts with UL20 and is required for infectious virus production. Virology. 2016;499:156-164.

LEGEND OF FIGURES

Figure 1. BoHV-1 efficiently targets HMCLs and induces cytotoxicity.

A) Flow cytometry histograms showing the expression levels of CD111, CD155, and CD138 in JJN-3, MM.1S, and OPM-2 cells. **B)** Assessment of cell mortality in JJN-3, MM.1S, and OPM-2 following BoHV-1 infection at 1 and 2 MOI for 24 h, 48 h, and 72 h.

Each dot represents an independent experiment (n=4); bars indicate mean ± SD. Statistical significance was determined using two-way ANOVA with Tukey's multiple comparisons test. $^{**}p < 0.01$, $^{***}p < 0.001$, $^{****}p < 0.0001$

Figure 2. BoHV-1 triggers apoptotic and transcriptional reprogramming in HMCLs.

A) Percentage of APO2.7$^+$ apoptotic cells in JJN-3, MM.1S, and OPM-2 cells at the indicated time points following BoHV-1 infection (1 and 2 MOI). Data represent means ± SD from four independent experiments. Statistical significance was determined using two-way ANOVA with Tukey's multiple comparisons test. **B)** Immunoblot analysis of pro- and cleaved caspase-3 in JJN-3, MM.1S, and OPM-2 cells treated with or without BoHV-1 (1 and 2 MOI) for 48 h. Vinculin serves as a loading control. **C)** Volcano plot of differentially expressed genes in JJN-3 cells infected with BoHV-1 (1 MOI, 24 h) compared to untreated cells. Genes were considered significantly upregulated if log2(Fold change) > 1 and FDR < 0.0005 (red), significantly downregulated if log2(Fold change) < -1 and FDR < 0.0005 (blue), and non-significant genes in grey. **D)** GSEA showing the top 10 significantly enriched upregulated and downregulated hallmark gene sets in JJN-3 cells infected with BoHV-1 (1 MOI, 24 h). Hallmark gene sets were considered significantly enriched at FDR < 0.05. $^{**}p < 0.01$, $^{***}p < 0.001$, $^{****}p < 0.0001$

Figure 3. BoHV-1 induces cytotoxicity in malignant PCs within patient-derived BM cells.

A) Scatter plots show CD111, CD155, and CD138 MFI across BMMC populations (n=25 patients per population; n=7 for HSPCs). **B)** Relative viability of purified MM CD138$^+$ PCs (n=6), infected with

BoHV-1 at 1 and 2 MOI for 48 h, 72 h, and 96 h vs untreated samples. **C)** Relative viability of PCs in total BMMCs from MM patients treated with BoHV-1 (1 and 2 MOI), for 48 h, 72 h, and 96 h vs the untreated samples. Results were pooled from 32, 30, and 24 patients, respectively.

Each dot represents an individual patient. Bars and boxplots indicate medians with IQR; lines connect paired samples where applicable. Statistical analyses were performed using two-way ANOVA with Tukey's multiple comparisons test **(B)** and Friedman test with Dunn's multiple comparisons test **(C)**. *$p < 0.05$, ***$p < 0.001$, ****$p < 0.0001$

Figure 4. Tumor-burden-independent PC cytotoxicity and selective BM remodeling by BoHV-1.

A) Correlation between baseline PC percentage in untreated BMMCs and PC viability after 96 h of BoHV-1 infection at 2 MOI (n=25). **B**) Comparison of 96 h PC viability following BoHV-1 infection (2 MOI) between NDMM (n=17) and RRMM (n=7) patients. **C)** Comparison of 96 h PC viability following BoHV-1 infection (2 MOI) between SRMM (n=11) and HRMM (n=13) patients. **D)** Percentage of cell populations within non-tumor BM cells (HSPCs, T cells, NK cells, B cells, and myeloid cells) after 96 h of BoHV-1 treatment (1 and 2 MOI) compared to untreated controls (results pooled from 15 patients for HSPCs and 23 patients for all other cell populations).

Each dot represents an individual patient. Bars and boxplots indicate medians with IQR; lines connect paired samples where applicable. Statistical analyses were performed using the Friedman test with Dunn's multiple comparisons test **(D)**, Spearman's rank correlation test **(A)**, and Mann-Whitney test **(B, C)**. **$p < 0.01$, ***$p < 0.001$, ****$p < 0.0001$

Figure 5. BoHV-1 enhances the activation of immune effector cells and promotes the expression of immunogenic markers in MM cells.

A) Relative CD69 expression on $CD8^+$ T cells from MM patients' BMMCs (n=18) treated with BoHV-1 (1 and 2 MOI) for 18 h vs the untreated samples. **B)** Percentages of $CD107a^+$ on $CD8^+$ T cells among BMMCs (n=18) after 18 h of treatment. **C)** Relative CD69 expression on NK cells

among BMMCs at 18 h and **D)** relative CD38 expression on the same population at 48 h following BoHV-1 treatment (1 and 2 MOI), compared to untreated samples (results pooled from 18 patients for CD69 and 26 patients for CD38). **E)** Percentages of $CD107a^+$ on NK cells among BMMCs (n=18) after 18 h of treatment. **F)** Heatmap of the top 25 up- and downregulated genes in the KEGG "Natural killer cell-mediated cytotoxicity" pathway from bulk RNA-seq of JJN-3 cells treated with BoHV-1 (1 MOI) for 24 h or untreated (n=3 per group). Data were processed and visualized in R; the color scale represents Z-scores. **G)** NK-92-mediated cytotoxicity of JJN-3 cells, untreated or pre-treated with BoHV-1 (1 MOI, 24 h), assessed after 4 h co-culture at increasing E:T ratios across three independent experiments. Data are shown as means ± SD.

Each dot represents an individual patient. Bars and boxplots indicate medians with IQR; lines connect paired samples where applicable. Statistical analyses were performed using two-way ANOVA with Tukey's multiple comparisons test (**G)** and Friedman test with Dunn's multiple comparisons test **(A-E)**. $^{**}p < 0.01$, $^{***}p < 0.001$, $^{****}p < 0.0001$

Figure 6. BoHV-1 reduces suppressive myeloid subsets, activates mono/macrophages, and induces a pro-inflammatory cytokine milieu.

A) Percentages of $CD11b^+CD14^-$ and $CD11b^+CD14^{dim/+}$ myeloid subsets among non-tumor cells from MM patients' BMMCs (n=22) after 96 h of BoHV-1 treatment. **B)** Relative frequencies of $CD16^+$ and $CD16^-$ cells within the $CD11b^+CD14^-$ compartment from MM patients' BMMCs (n=9) after 96 h of BoHV-1 treatment. **C)** Relative CD69 expression on $CD11b^+CD14^{dim/+}$ mono/macrophages among BMMCs at 18 h and **D)** relative CD38 expression on the same population at 48 h following BoHV-1 treatment (1 and 2 MOI), compared to untreated samples (results pooled from 18 patients for CD69 and 26 patients for CD38). **E)** Percentages of the $CD14^+CD16^-$ and $CD14^+CD16^+$ subsets among non-tumor cells from MM patients' BMMCs (n=32), untreated or treated with BoHV-1 (1 and 2 MOI) for 48 h. **F)** Relative cell viability of PCs in total

and monocyte-depleted BMMCs from MM patients (n=6) following BoHV-1 treatment at 1 and 2 MOI for 96h vs matched untreated samples. **G)** IFN-α, TNF-α, and IFN-γ levels in the cell-free supernatants of MM patients' BMMCs (n=8) treated with or without BoHV-1 (1 and 2 MOI for 48 h). Triangles indicate values exceeding the assay's detection limit; these were assigned the maximum detectable concentration and are therefore underestimated.

Each dot represents an individual patient. Bars and boxplots indicate medians with IQR; lines connect paired samples where applicable. Statistical analyses were performed using the Friedman test with Dunn's multiple comparisons test. *$p < 0.05$, **$p < 0.01$, ***$p < 0.001$, ****$p < 0.0001$

Figure 7. Combination treatments with BoHV-1 and standard anti-MM agents reduce tumor cell viability in patient-derived BMMCs.

B) Relative viability of PCs from MM patients' BMMCs (n=11) 96 h after treatment with BoHV-1 (1 and 2 MOI), BTZ (2 nM), alone or in combination. **B)** Relative viability of PCs from MM patients' BMMCs (n=9) 96 h after treatment with BoHV-1 (1 and 2 MOI), LENA (10 µM), alone or in combination. **C)** Relative CD38 expression on PCs from MM patients' BMMCs (n=34) after 48 h of treatment. **D)** Experimental design for BoHV-1 and DARA combination. **E)** Relative viability of PCs from MM patients' BMMCs (n=12) 96 h after treatment with BoHV-1 (1 and 2 MOI), DARA (10 µg/mL), alone or in combination.

All treatments were compared to untreated controls. Data from patient-derived BMMCs are presented as median with IQR from paired experiments. Black dots represent patients with NDMM, while red dots represent those with RRMM. Statistical analysis was performed using the Friedman test with Dunn's correction. *$p < 0.05$, **$p < 0.01$, ***$p < 0.001$, ****$p < 0.0001$

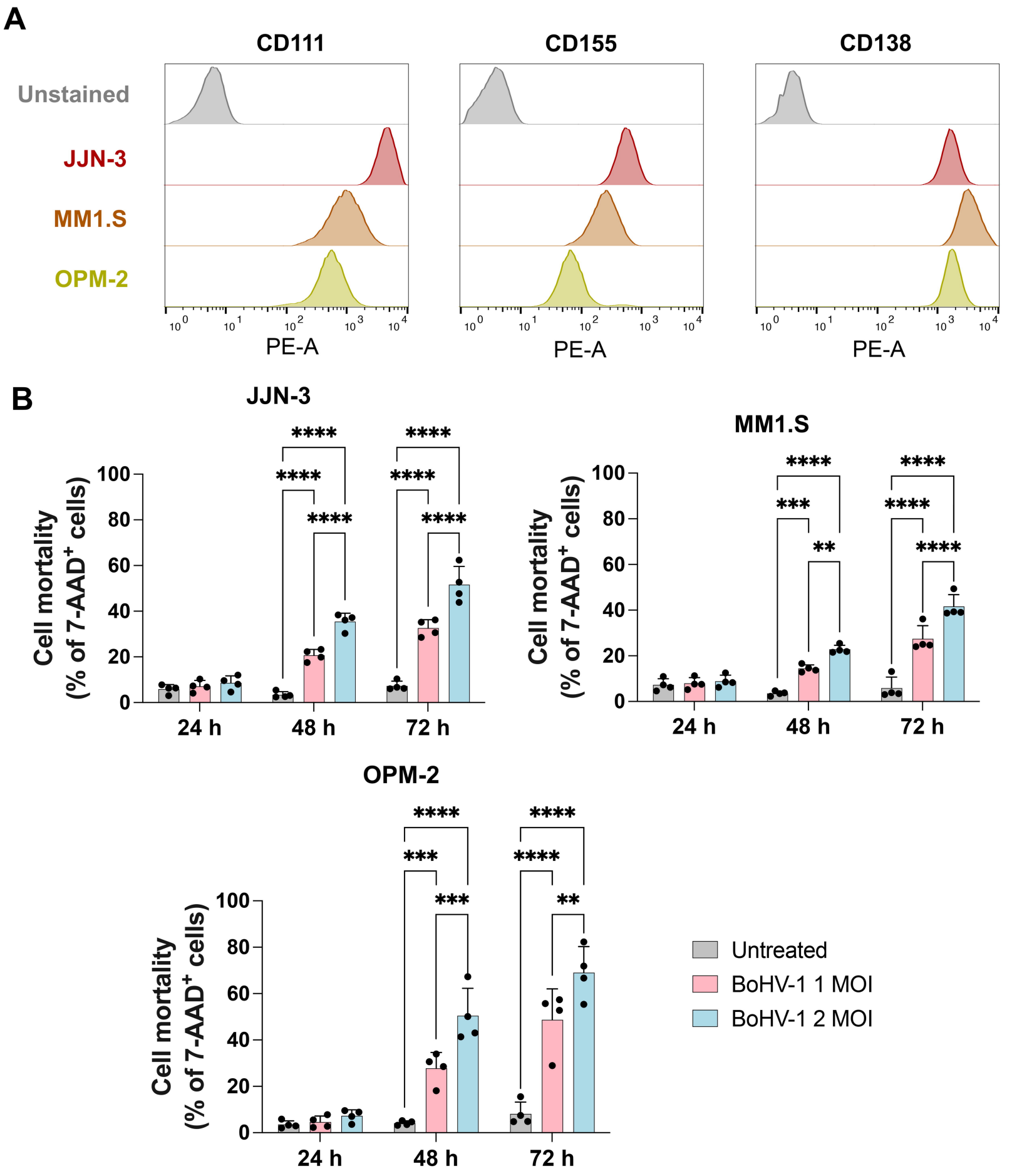
A
CD111
CD155
CD138
Unstained
JJN-3
MM1.S
OPM-2
PE-A
B
JJN-3
MM1.S
OPM-2
Cell mortality
(% of 7-AAD+ cells)
24 h
48 h
72 h
Untreated
BoHV-1 1 MOI
BoHV-1 2 MOI

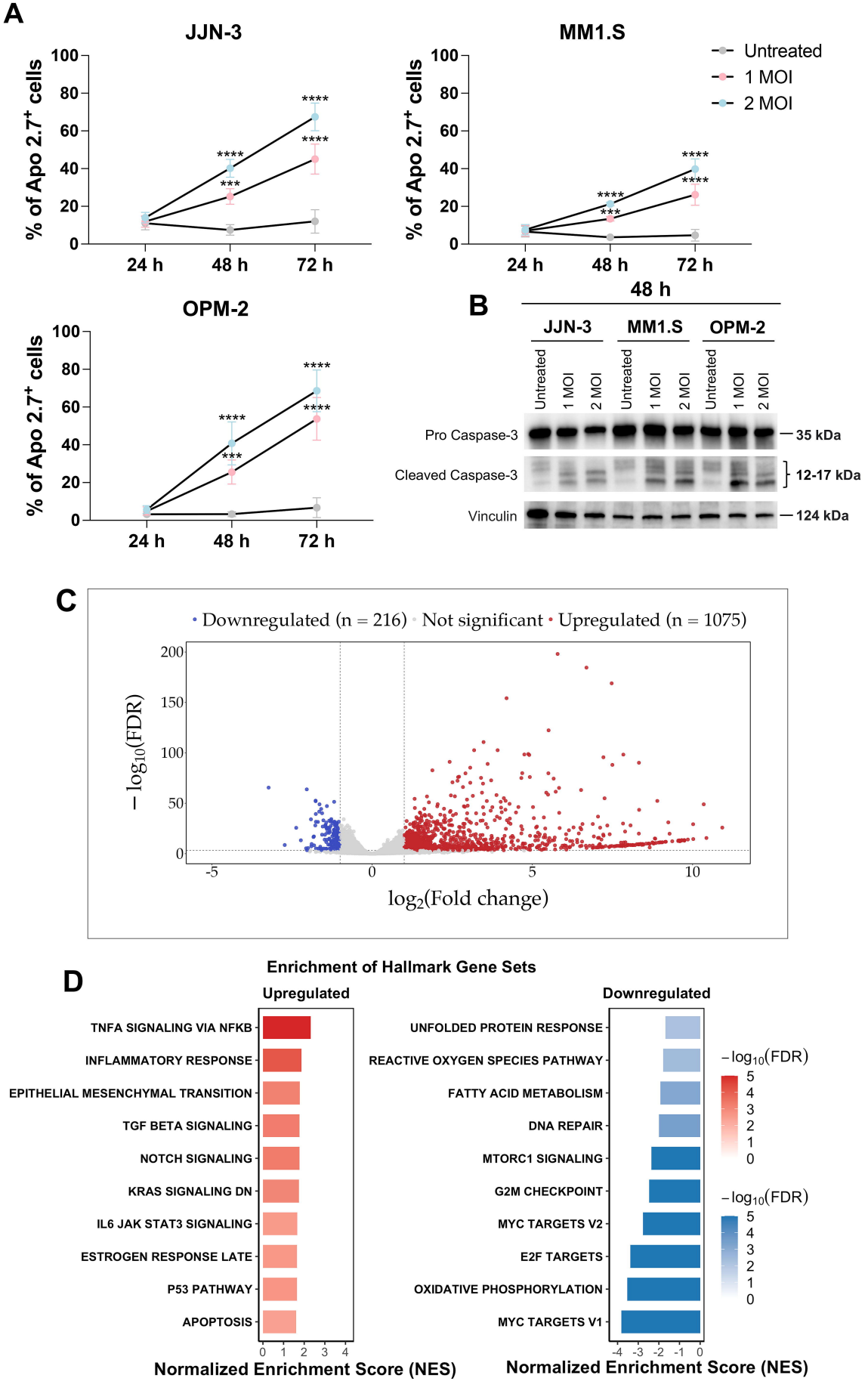
A
JJN-3
MM1.S
OPM-2
% of Apo 2.7+ cells
Untreated
1 MOI
2 MOI
24 h
48 h
72 h
B
48 h
JJN-3
MM1.S
OPM-2
Pro Caspase-3
Cleaved Caspase-3
Vinculin
35 kDa
12-17 kDa
124 kDa
C
Downregulated (n = 216)
Not significant
Upregulated (n = 1075)
−log10(FDR)
log2(Fold change)
D
Enrichment of Hallmark Gene Sets
Upregulated
TNFA SIGNALING VIA NFKB
INFLAMMATORY RESPONSE
EPITHELIAL MESENCHYMAL TRANSITION
TGF BETA SIGNALING
NOTCH SIGNALING
KRAS SIGNALING DN
IL6 JAK STAT3 SIGNALING
ESTROGEN RESPONSE LATE
P53 PATHWAY
APOPTOSIS
Normalized Enrichment Score (NES)
Downregulated
UNFOLDED PROTEIN RESPONSE
REACTIVE OXYGEN SPECIES PATHWAY
FATTY ACID METABOLISM
DNA REPAIR
MTORC1 SIGNALING
G2M CHECKPOINT
MYC TARGETS V2
E2F TARGETS
OXIDATIVE PHOSPHORYLATION
MYC TARGETS V1
Normalized Enrichment Score (NES)
−log10(FDR)
−log10(FDR)

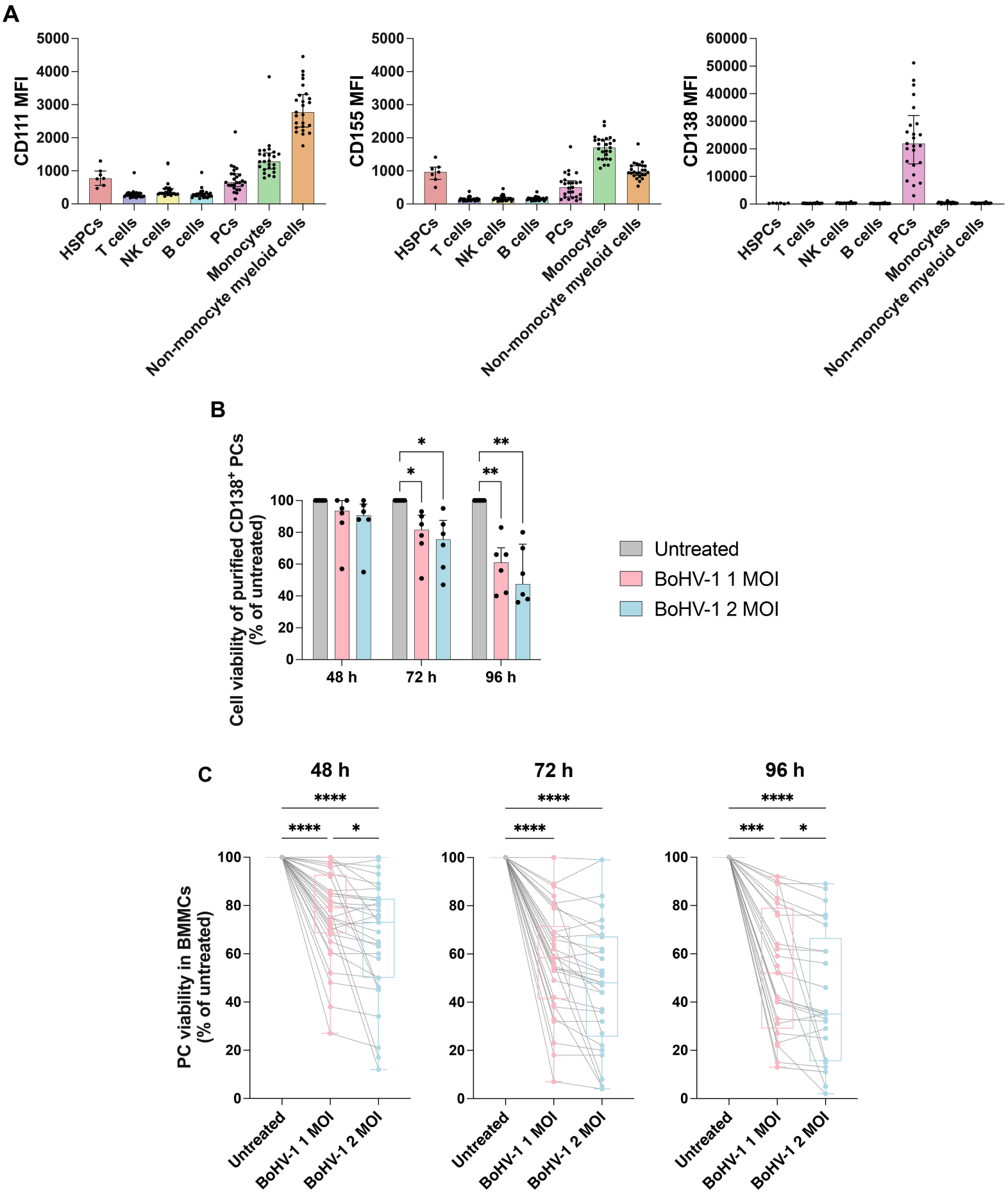
A
CD111 MFI
CD155 MFI
CD138 MFI
HSPCs
T cells
NK cells
B cells
PCs
Monocytes
Non-monocyte myeloid cells
B
Cell viability of purified CD138+ PCs (% of untreated)
48 h
72 h
96 h
Untreated
BoHV-1 1 MOI
BoHV-1 2 MOI
C
PC viability in BMMCs (% of untreated)

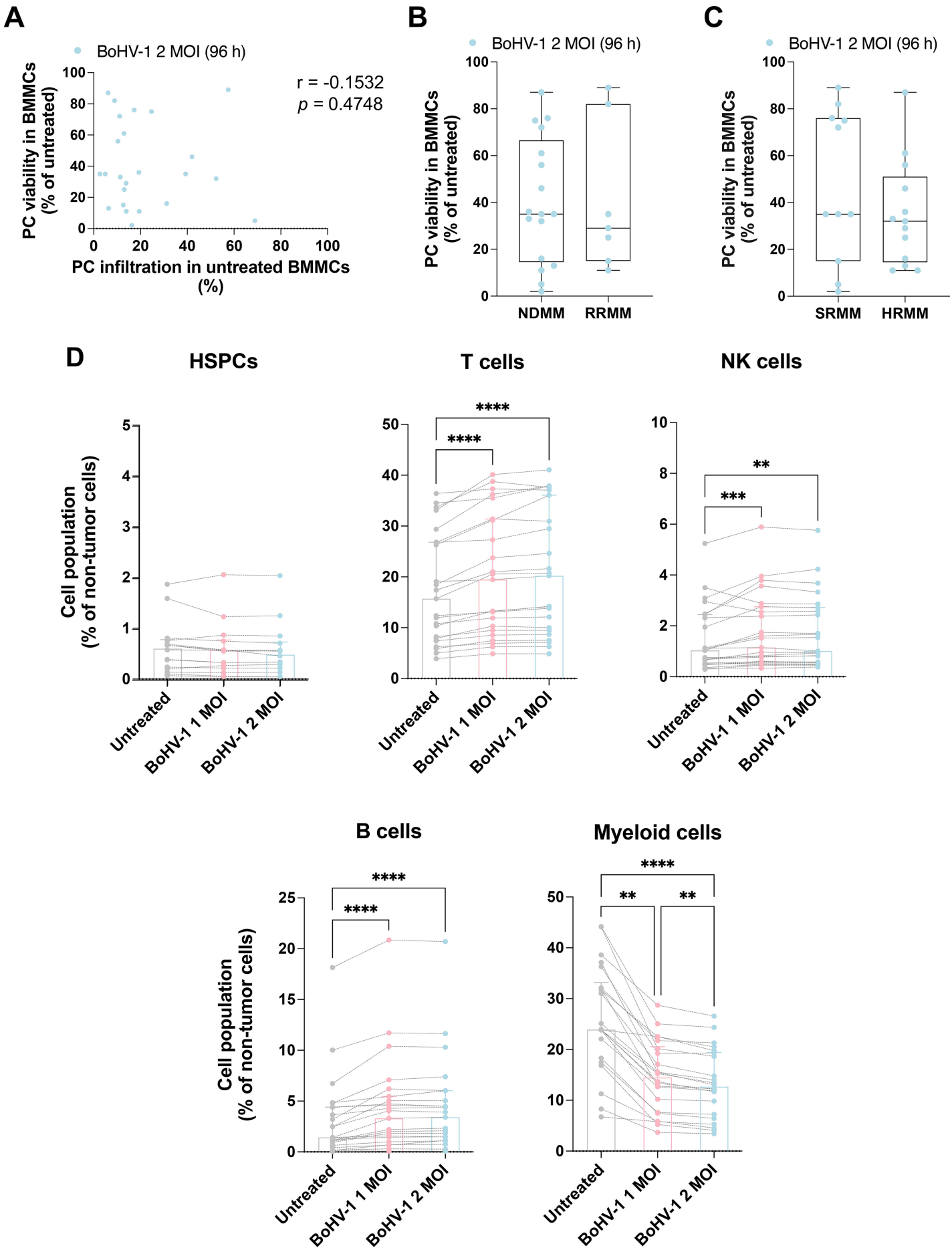
A
BoHV-1 2 MOI (96 h)
r = -0.1532
p = 0.4748
PC viability in BMMCs (% of untreated)
PC infiltration in untreated BMMCs (%)
B
BoHV-1 2 MOI (96 h)
PC viability in BMMCs (% of untreated)
NDMM
RRMM
C
BoHV-1 2 MOI (96 h)
PC viability in BMMCs (% of untreated)
SRMM
HRMM
D
HSPCs
T cells
NK cells
B cells
Myeloid cells
Cell population (% of non-tumor cells)
Untreated
BoHV-1 1 MOI
BoHV-1 2 MOI
****
**
***

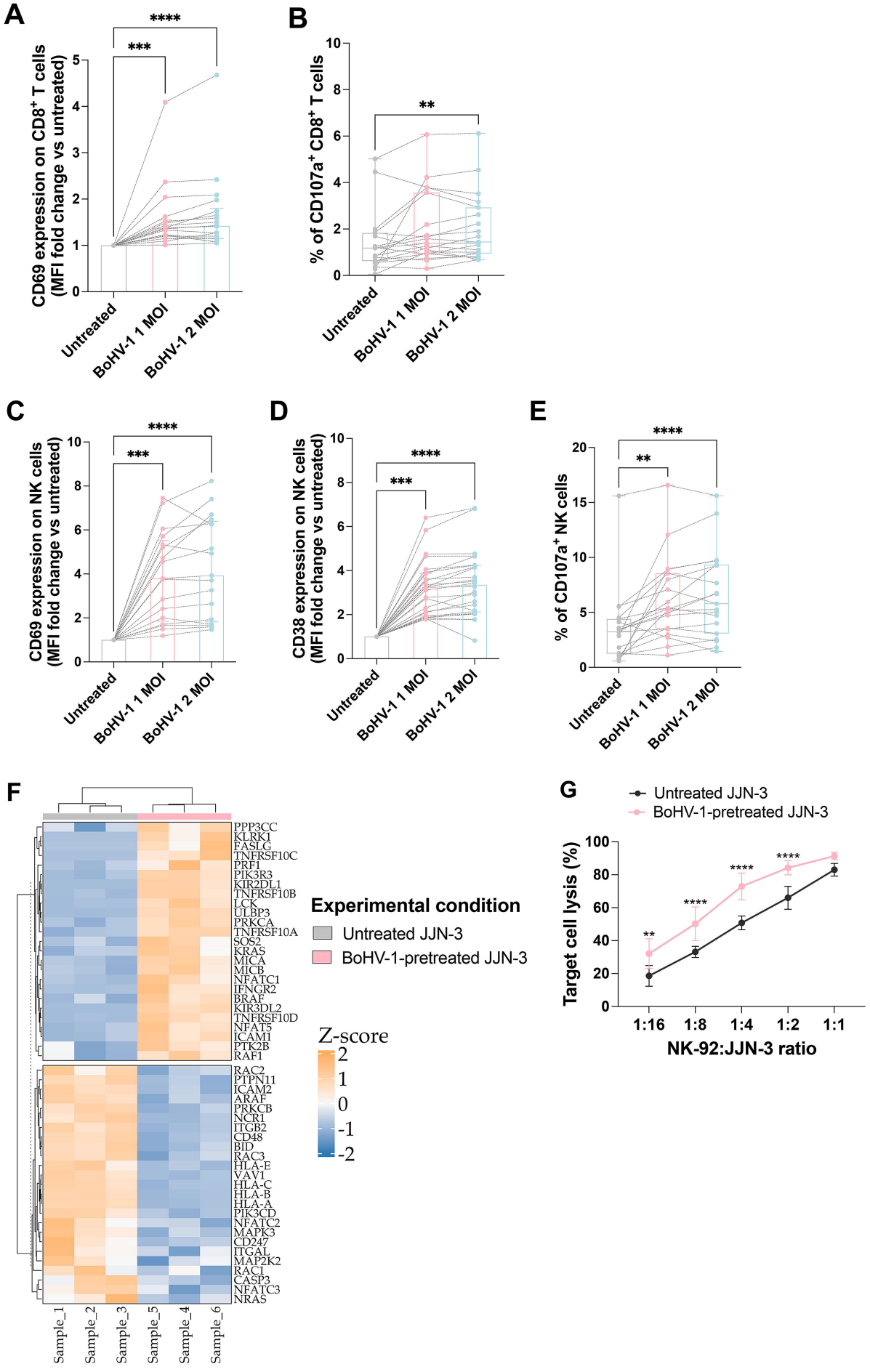
A
CD69 expression on CD8+ T cells (MFI fold change vs untreated)
Untreated
BoHV-1 1 MOI
BoHV-1 2 MOI
B
% of CD107a+ CD8+ T cells
C
CD69 expression on NK cells (MFI fold change vs untreated)
D
CD38 expression on NK cells (MFI fold change vs untreated)
E
% of CD107a+ NK cells
F
PPP3CC
KLRK1
FASLG
TNFRSF10C
PRF1
PIK3R3
KIR2DL1
TNFRSF10B
LCK
ULBP3
PRKCA
TNFRSF10A
SOS2
KRAS
MICA
MICB
NFATC1
IFNGR2
BRAF
KIR3DL2
TNFRSF10D
NFAT5
ICAM1
PTK2B
RAF1
RAC2
PTPN11
ICAM2
ARAF
PRKCB
NCR1
ITGB2
CD48
BID
RAC3
HLA-E
VAV1
HLA-C
HLA-B
HLA-A
PIK3CD
NFATC2
MAPK3
CD247
ITGAL
MAP2K2
RAC1
CASP3
NFATC3
NRAS
Sample_1
Sample_2
Sample_3
Sample_5
Sample_4
Sample_6
Experimental condition
Untreated JJN-3
BoHV-1-pretreated JJN-3
Z-score
G
Untreated JJN-3
BoHV-1-pretreated JJN-3
Target cell lysis (%)
NK-92:JJN-3 ratio
1:16
1:8
1:4
1:2
1:1

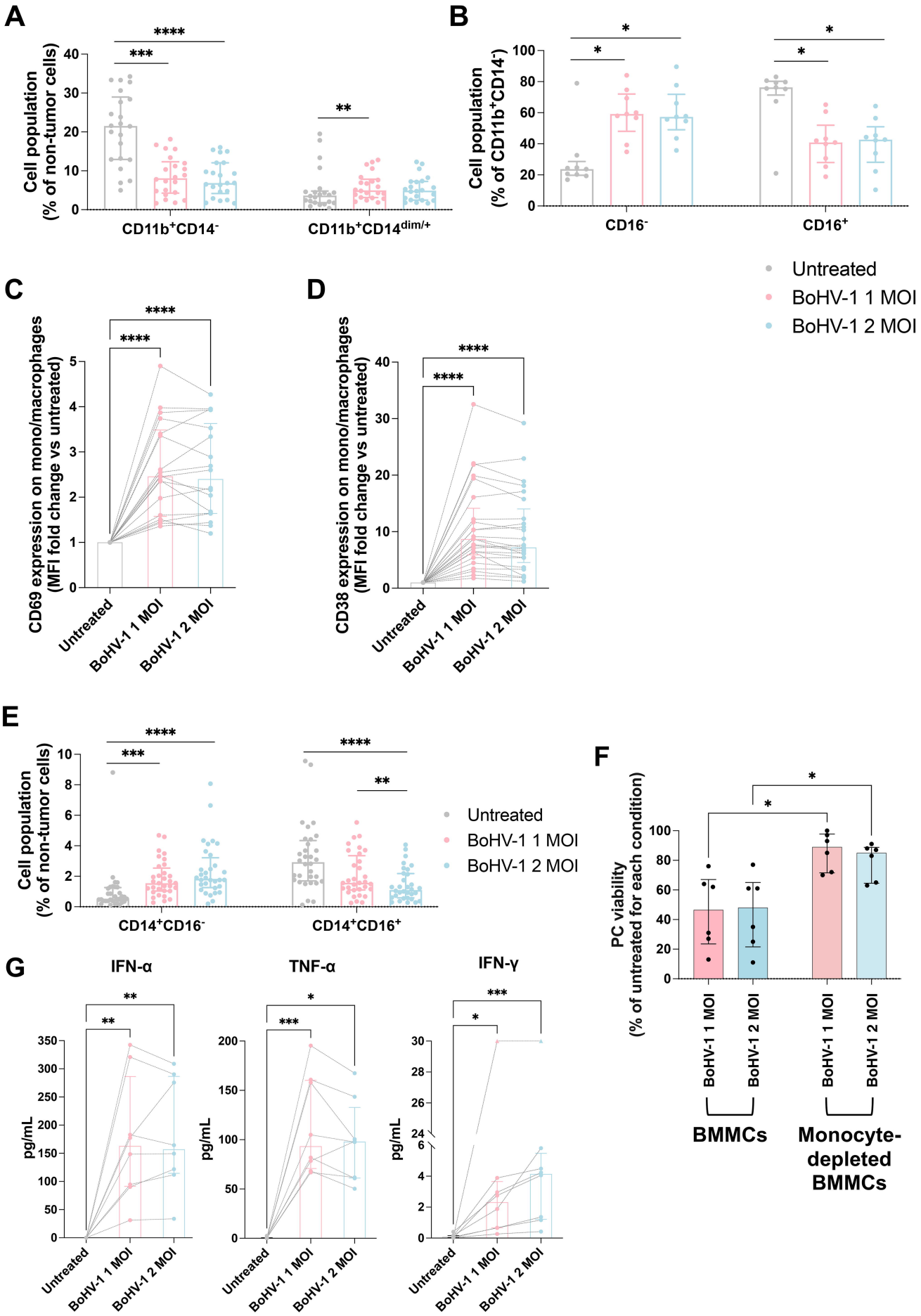
A
Cell population (% of non-tumor cells)
CD11b+CD14-
CD11b+CD14dim/+
B
Cell population (% of CD11b+CD14-)
CD16-
CD16+
Untreated
BoHV-1 1 MOI
BoHV-1 2 MOI
C
CD69 expression on mono/macrophages (MFI fold change vs untreated)
D
CD38 expression on mono/macrophages (MFI fold change vs untreated)
E
Cell population (% of non-tumor cells)
CD14+CD16-
CD14+CD16+
F
PC viability (% of untreated for each condition)
BMMCs
Monocyte-depleted BMMCs
G
IFN-α
TNF-α
IFN-γ
pg/mL

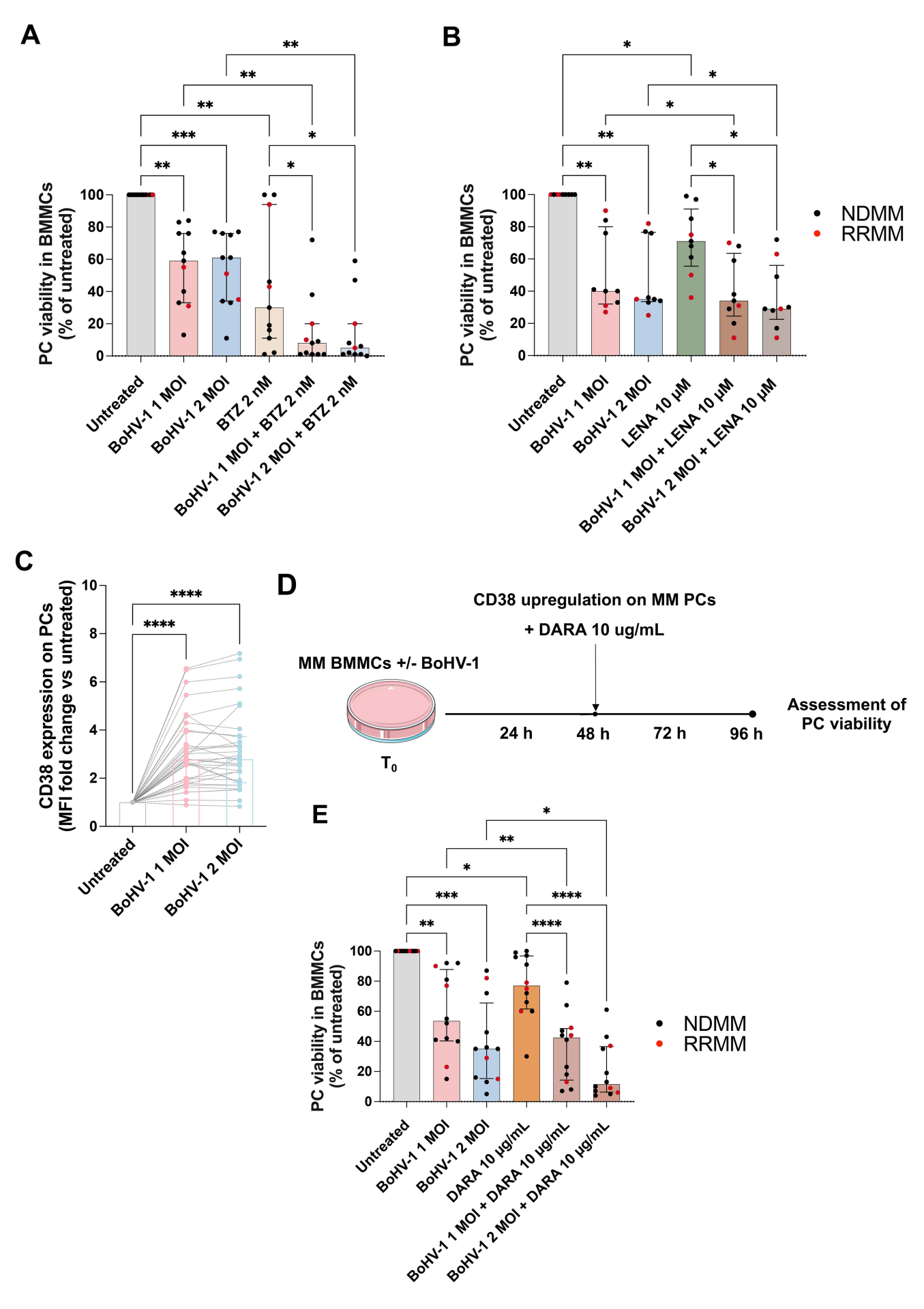
A
PC viability in BMMCs (% of untreated)
Untreated
BoHV-1 1 MOI
BoHV-1 2 MOI
BTZ 2 nM
BoHV-1 1 MOI + BTZ 2 nM
BoHV-1 2 MOI + BTZ 2 nM
B
PC viability in BMMCs (% of untreated)
NDMM
RRMM
Untreated
BoHV-1 1 MOI
BoHV-1 2 MOI
LENA 10 µM
BoHV-1 1 MOI + LENA 10 µM
BoHV-1 2 MOI + LENA 10 µM
C
CD38 expression on PCs (MFI fold change vs untreated)
Untreated
BoHV-1 1 MOI
BoHV-1 2 MOI
D
CD38 upregulation on MM PCs
+ DARA 10 ug/mL
MM BMMCs +/- BoHV-1
T0
24 h
48 h
72 h
96 h
Assessment of PC viability
E
PC viability in BMMCs (% of untreated)
NDMM
RRMM
Untreated
BoHV-1 1 MOI
BoHV-1 2 MOI
DARA 10 µg/mL
BoHV-1 1 MOI + DARA 10 µg/mL
BoHV-1 2 MOI + DARA 10 µg/mL

Oncolytic bovine herpesvirus type 1 induces immune microenvironment remodeling and enhances treatment responses in multiple myeloma

Vincenzo Raimondi[1], Rosanna Vescovini[1], Paola Storti[1], Valentina Franceschi[2], Giulia Pozzi[1], Camilla Sitzia[1], Nicolas Thomas Iannozzi[1], Denise Toscani[1,3], Benedetta Dalla Palma[3], Matteo Scita[3], Mattia Dessena[1], Sergio Minesso[2], Stefania Ricci[1], Fazel Mohammadi[1], Oxana Lungu[1], Prisco Mirandola[1], Gaetano Donofrio[2] and Nicola Giuliani[1,3]

[1]Department of Medicine and Surgery, University of Parma, Parma, Italy.

[2]Department of Medical-Veterinary Science, University of Parma, Parma, Italy.

[3]Hematology, "Azienda Ospedaliero-Universitaria di Parma", Parma, Italy.

SUPPLEMENTARY INFORMATION

SUPPLEMENTARY METHODS

Cell lines and reagents

Cell lines: The bovine embryo kidney cell line (BS CL-94; BEK) was kindly provided by M. Ferrari (Istituto Zooprofilattico Sperimentale, Brescia, Italy). The Madin-Darby bovine kidney cell line (MDBK; ATCC CCL-22) was obtained from ATCC (Manassas, VA, USA). Cells were maintained in Eagle's Minimal Essential Medium (EMEM) supplemented with 10% heat-inactivated fetal bovine serum (FBS), sodium pyruvate (1 mM), L-glutamine (2 mM), amphotericin B (0.25 μg/mL), and antibiotics (100 U/mL penicillin and 100 μg/mL streptomycin) (all from Gibco, Segrate, Italy). The human myeloma cell lines (HMCLs) JJN-3, MM1.S, and OPM-2 were purchased from the Leibniz Institute Deutsche Sammlung von Mikroorganismen und Zellkulturen GmbH (Braunschweig, Germany). Cells were maintained in Roswell Park Memorial Institute (RPMI) 1640 medium supplemented with 10% heat-inactivated FBS, L-glutamine (2 mM), amphotericin B (0.25 μg/mL), and antibiotics (100 U/mL penicillin and 100 μg/mL streptomycin) (ThermoFisher Scientific, Monza, Italy). The human stromal cell line HS-5 was purchased from ATCC (Manassas, VA, USA) and cultured in Dulbecco's Modified Eagle Medium (DMEM) supplemented with the same supplements.

The human NK-92 cell line, an interleukin-2 (IL-2)-dependent natural killer cell line, was obtained from ATCC (Manassas, VA, USA). Cells were cultured in α-MEM supplemented with 12.5% heat-inactivated horse serum, 12.5% heat-inactivated FBS, L-glutamine (2 mM), amphotericin B (0.25 μg/mL), and antibiotics (100 U/mL penicillin and 100 μg/mL streptomycin), and 100 U/mL recombinant human IL-2 (all from ThermoFisher Scientific, Monza, Italy).

All the cultures were incubated at 37 °C in a humidified atmosphere containing 5% CO_2.

Bovine virus: Bovine herpesvirus type 1 (BoHV-1) wild-type (Cooper strain (Colorado-1), ATCC) was propagated by infecting confluent monolayers of BEK or MDBK cells at a multiplicity of infection (MOI) of 0.1 50% tissue culture infectious doses ($TCID_{50}$) per cell. Cells were maintained in EMEM supplemented with 2% heat-inactivated FBS for 2 h. The medium was then removed and replaced with fresh EMEM containing 10% FBS. When cytopathic effect affected the majority of the cell monolayer (approximately 48 h post-infection), the virus was harvested by freezing and thawing the cells three times and pelleting the virions through a 30% sucrose gradient, as previously described.[29] Virus pellets were resuspended in cold EMEM without FBS. $TCID_{50}$ was determined in BEK or MDBK cells by limiting dilution. For control experiments, BoHV-1 was heat-inactivated by incubation at 95 °C for 1 h.

Drugs: Bortezomib (BTZ; Selleckchem, Munich, Germany), lenalidomide (LENA; Celgene, Milan, Italy), daratumumab (DARA; Janssen Biotech, USA), and elranatamab (ELRA; MedChemExpress, USA) were reconstituted according to the manufacturers' instructions and diluted in culture medium immediately before use.

Patient samples and cell isolation

Bone marrow (BM) aspirates were processed within 4 h of collection. BM mononuclear cells (BMMCs) were obtained from BM aspirates by Ficoll-Hypaque (Bichrome AG, Berlin, Germany) density gradient sedimentation and cultured in RPMI 1640 medium supplemented with 20% heat-inactivated FBS, L-glutamine (2 mM), amphotericin B (0.25 µg/mL), and antibiotics (100 U/mL penicillin and 100 µg/mL streptomycin) (ThermoFisher Scientific, Monza, Italy). Fresh BMMCs were used to preserve cellular subset integrity and viability, with particular attention to myeloid populations, which are highly susceptible to freeze-thaw-induced perturbations.

$CD138^+$ cells were purified from the BMMCs of multiple myeloma (MM) patients by antibody-mediated positive selection using anti-CD138 magnetic-activated cell separation microbeads

(Miltenyi Biotec, Gladbach, Germany). The purity of immunoselected cells was assessed by flow cytometry analysis using a PE-conjugated anti-CD138 monoclonal antibody. Purified $CD138^+$ cells were seeded and cultured in RPMI 1640 medium supplemented with 20% heat-inactivated FBS, L-glutamine (2 mM), amphotericin B (0.25 µg/mL), and antibiotics (100 U/mL penicillin and 100 µg/mL streptomycin) (ThermoFisher Scientific, Monza, Italy).

Monocytes were removed from BMMCs by antibody-mediated positive selection using anti-CD14 magnetic-activated cell separation microbeads (Miltenyi Biotec, Gladbach, Germany). The $CD14^-$ fraction (monocyte-depleted BMMCs) was seeded and cultured as described. Depletion efficiency was confirmed by flow cytometry using an anti-CD14 BV786 antibody.

Virus and drug treatments

The HMCLs and the human stromal cell line HS-5 were cultured with or without BoHV-1 for 24 h, 48 h, or 72 h. BoHV-1 was used at 1 and 2 MOI per $1x10^6$ cells. At the end of the experiments, cells were collected for flow cytometry analysis. For transcriptomic analysis, JJN-3 cells were infected with BoHV-1 at 1 MOI and incubated for 24 h. Afterward, the cells were harvested, washed with PBS, and lysed in RLT buffer (Qiagen, Hilden, Germany) for RNA extraction and RNA sequencing.

JJN-3 cells were also treated with BTZ (2, 3, or 5 nM) or LENA (1, 2, or 10 µM), as a single agent or administered concurrently with BoHV-1 (1 MOI) and incubated for 72 h. The MTT assay was used to assess the effect of treatments.

$CD138^+$ purified from BMMCs of MM patients ($0,25x10^6$ cells) were cultured with or without BoHV-1 at 1 and 2 MOI for 48 h, 72 h, or 96 h. After treatment, cells were harvested and analyzed using flow cytometry.

BMMCs from MM patients ($1x10^6$ cells) were cultured with or without BoHV-1 at 1 and 2 MOI for 48 h, 72 h, or 96 h. After treatment, all cells were harvested, washed, and analyzed using flow

cytometry. Cell-free supernatants from the culture were harvested by 8 minutes of centrifugation at 400 × g, aliquoted, and stored at -20 °C until use.

For combination experiments, BMMCs were treated with or without BoHV-1 at 1 and 2 MOI, either alone or in combination with BTZ (2 nM) or LENA (10 µM), both added at the time of infection. To explore combinations with antibody-based therapies, cells were first treated with BoHV-1, and then, 24 h or 48 h after viral exposure, ELRA (0.01 nM) or DARA (10 µg/mL) was administered, respectively. Cells were maintained in culture for a total of 96 h, after which they were harvested and analyzed by flow cytometry.

In vitro blockade of CD111, CD155, and CD138 receptors during BoHV-1 infection

MM1.S ($1x10^6$ cells) were pre-incubated for 1 h with or without 2 µL of each blocking antibody against CD111, CD155, and CD138 (all purchased from BioLegend, San Diego, CA, USA) in dual (CD111 and CD155) or triple (CD111, CD155, and CD138) combinations. Cells were then plated and treated with BoHV-1 at 1 MOI or left untreated. After 48 h, all cells were harvested and analyzed using flow cytometry.

NK cell-mediated cytotoxicity assay

NK-92 cell-mediated cytotoxicity was assessed following pre-treatment of target cells with BoHV-1. JJN-3 cells were infected with BoHV-1 for 24 h, washed extensively to remove residual virus, and then stained with 10nM of calcein-AM (Sigma-Aldrich, St. Louis, MO, USA) for 30 minutes at 37 °C. After incubation, JJN-3 cells were washed and co-cultured with NK-92 effector cells at the indicated effector-to-target (E:T) ratio for 4 h. At the end of co-culture, cells were harvested, stained with 5 µL of anti-CD56 PE-conjugated antibody (Beckman Coulter, Brea, CA, USA) to discriminate NK-92 cells ($CD56^+$) from JJN-3 target cells ($CD56^-$), and analyzed by flow cytometry. Cytotoxicity was determined by quantifying the percentage of JJN-3 cells ($CD56^-$) that were negative for calcein-AM fluorescence, indicating loss of membrane integrity.

Normalized cytotoxicity (%) was calculated using the following formula: [(cytotoxicity in co-culture - spontaneous cytotoxicity in monoculture) / (100 - spontaneous cytotoxicity in monoculture)] × 100.

Cytokine detection by ELISA

Cytokines were measured in the cell-free supernatants of BMMCs treated with or without BoHV-1, as described above. Levels of IFN-α, TNF-α, IFN-γ, IL-6, and IL-1β were determined using commercial ELISA kits (Human IFN-α All Subtype ELISA Kit, Human TNF-α Quantikine HS ELISA Kit, Human IFN-γ Quantikine HS ELISA Kit, Human IL-6 Quantikine HS ELISA Kit, and Human IL-1 beta/IL-1F2 Quantikine HS ELISA Kit; all from R&D Systems, Minneapolis, MN, USA), according to the manufacturers' protocols. Absorbance was measured at 450 nm with wavelength correction at 540 nm using a microplate reader. Cytokine levels were determined from standard curves included in each assay.

Flow cytometry

For all flow cytometry procedures, sample acquisition was performed using a two-laser FACSCelesta cytometer equipped with FACSDiva Software (v8.02; BD Biosciences, Franklin Lakes, NJ, USA), and data were analyzed and plotted using FlowJo Software (v10; BD Biosciences, Franklin Lakes, NJ, USA). Single-fluorochrome compensation was carried out using BD CompBeads and patient-derived BMMCs. Protocols were optimized to minimize inter-patient variability. BD FACSDiva CS&T research beads were used to monitor and adjust photomultiplier tube settings over time. To ensure reproducibility, the same antibody lots were used for all patient samples, and a single operator performed gating and data analysis. All FACS plots were manually inspected to confirm staining quality and data acquisition integrity.

CD111, CD155, and CD138 expression: expression levels of CD111, CD155, and CD138 antigens were determined on HMCLs and HS-5 stromal cells by flow cytometry analysis and expressed as median fluorescence intensity (MFI). In particular, $0.2x10^6$ HMCLs or HS-5 stromal cells were stained in

parallel with either a saturating concentration of anti-CD111 (BioLegend, San Diego, CA, USA), anti-CD155 PE, or anti-CD138 BV421 (both BD Biosciences, Franklin Lakes, NJ, USA) for 30 minutes at 4 °C, protected from light. Cells were then washed with a washing buffer (PBS plus 5% human serum albumin and 5% w/v sodium azide) and directly analyzed by flow cytometry. Before the acquisition, the 7-Amino Actinomycin D (7-AAD) was added according to the manufacturer's instructions. After identification of singlets and exclusion of debris, viable cells were identified as 7-AAD$^-$ events in side scatter (SSC) vs 7-AAD plots. Unstained samples were used to define gating boundaries.

CD111, CD155, and CD138 expression levels on fresh BMMCs were detected by staining 0.5x10^6 cells/tube with a cocktail of saturating concentrations of antibodies in 50 µl of brilliant stain buffer (BD Biosciences, Franklin Lakes, NJ, USA) and 50 µl of washing buffer supplemented with 10% of mouse serum. The antibodies (all, except anti-CD111, purchased from BD Biosciences, Franklin Lakes, NJ, USA) were combined in the two following panels: (1) anti-CD138 BV421, anti-CD38 BV480, anti-CD3 BV605, anti-CD16 BV650, anti-CD56 BV711, anti-CD14 BV786, anti-CD11b FITC, anti-CD111 or anti-CD155 PE, and anti-CD19 PE-CF594; (2) anti-CD138 BV421, anti-CD38 BV480, anti-CD3 BV605, anti-CD16 BV650, anti-CD56 BV711, anti-CD14 BV786, anti-CD34 FITC, anti-CD111 or anti-CD155 PE, and anti-CD19 PE-CF594. Fluorescence-minus-one (FMO) controls were used to define PE gating boundaries. After incubation for 30 minutes at 4 °C protected from light, BMMCs were washed with the washing buffer. Before flow cytometry acquisition, 7-AAD was added according to the manufacturer's instructions. Then, viable cells were identified as 7-AAD$^-$ events, and CD111 or CD155 expression levels were determined on specific gates identifying hematopoietic stem and progenitor cells (HSPCs) (CD34$^+$), T cells (CD3$^+$), NK cells (CD3$^-$CD16$^+$CD56$^+$CD138$^-$), B cells (CD19$^+$), plasma cells (PCs) (CD138$^+$CD38$^+$), monocytes (CD11b$^+$CD14$^{dim/+}$) and non-monocyte myeloid cells (SSC^{high}CD11b$^+$CD14$^-$). The full gating strategy is provided in Supplementary Figure S1A.

Viability staining and apoptotic assay on cell lines: Untreated or BoHV-1-treated HMCLs and HS-5 stromal cells were stained, according to the manufacturer's instructions, with 7-AAD (BD Biosciences, Franklin Lakes, NJ, USA). After identification of singlets and exclusion of debris, viable and non-viable cells were identified as 7-AAD$^-$ or 7-AAD$^+$ events, respectively, in SSC vs 7-AAD plots. Apoptosis was assessed by the APO2.7 evaluation, which specifically detects 7A6, a 38-kDa mitochondrial membrane antigen expressed during apoptosis. After treatment, cells were collected, stained with a saturating concentration of PE-conjugated APO2.7 antibody (Beckman Coulter, Brea, CA, USA) for 30 minutes at 4 °C protected from light, and analyzed by flow cytometry.

Identification of BMMCs subsets: After treatments, BMMCs were collected, washed, and stained with a cocktail of saturating concentrations of antibodies in 50 µl of brilliant stain buffer (BD Biosciences, Franklin Lakes, NJ, USA) and 50 µl of washing buffer supplemented with 10% of mouse serum. The antibodies (all purchased from BD Biosciences, Franklin Lakes, NJ, USA) were combined in the following panel: anti-CD138 BV421, anti-CD38 BV480, anti-CD3 BV605, anti-CD16 BV650, anti-CD56 BV711, anti-CD14 BV786, anti-CD11b FITC, anti-CD34 PE, and anti-CD19 PE-CF594. After incubation for 30 minutes at 4 °C protected from light, BMMCs were washed with the washing buffer. Before flow cytometry acquisition, 7-AAD was added according to the manufacturer's instructions. PCs were identified as CD138$^+$CD38$^+$. Non-tumor cells, defined as those outside this gate, included HSPCs (CD34$^+$), T cells (CD3$^+$), NK cells (CD3$^-$CD16$^+$CD56$^+$), B cells (CD19$^+$), and myeloid cells (SSC^{high}CD11b$^+$CD14$^{-/+}$) were gated. The full gating strategy is provided in Supplementary Figure S1B.

The BoHV-1 oncolytic effect on PCs was calculated using the following formula: % of CD138$^+$CD38$^+$ cells normalized viability = (% of CD138$^+$CD38$^+$7-AAD$^-$ cells in the treated condition / % of CD138$^+$CD38$^+$7-AAD$^-$ cells in the untreated condition) x 100. In this calculation, the percentage of viable PCs in the untreated condition was set to 100%, and the viability of treated samples was

expressed relative to this value. This calculation was similarly applied to each non-tumor cell population.

Assessment of CD107a and CD69 expression: BMMCs ($1x10^6$ cells) were cultured with or without BoHV-1 at 1 and 2 MOI for 18 h. To assess degranulation, 1 µL of anti-CD107a PE (BD Biosciences, Franklin Lakes, NJ, USA) was added at the beginning of the culture. After treatment, BMMCs were washed and stained with a cocktail of saturating concentrations of antibodies (all purchased from BD Biosciences, Franklin Lakes, NJ, USA) combined in the following panel: anti-CD138 BV421, anti-CD38 BV480, anti-CD3 BV605, anti-CD16 BV650, anti-CD56 BV711, anti-CD14 BV786, anti-CD8 FITC, anti-CD19 PE-FC594. After incubation for 30 minutes at 4 °C protected from light, BMMCs were washed with the washing buffer. Before flow cytometry acquisition, 7-AAD was added according to the manufacturer's instructions. CD107a expression was evaluated on both $CD8^+$ T cells ($CD3^+CD8^+$) and NK cells ($CD3^-CD16^+CD56^+CD138^-$). For activation analysis, CD69 expression was assessed under the same culture conditions on $CD8^+$ T cells ($CD3^+CD8^+$), NK cells ($CD3^-CD16^+CD56^+CD138^-$), and mono/macrophages ($CD14^{dim/+}$). Anti-CD69 PE (BD Biosciences, Franklin Lakes, NJ, USA) was added at the end of the 18-h culture, together with the same antibody panel and staining protocol described above, including 7-AAD labeling before acquisition. The full gating strategy is provided in Supplementary Figure S2.

Bulk RNA sequencing

RNA isolation: Total cellular RNA was extracted from untreated and BoHV-1-treated JJN3 using the RNeasy Mini Kit (Qiagen, Hilden, Germany) according to the manufacturer's protocol. RNA quantity was measured with a NanoDrop One spectrophotometer (ThermoFisher Scientific, Monza, Italy), and RNA integrity was assessed using either the Agilent 2100 Bioanalyzer RNA assay or the TapeStation system (Agilent Technologies, Santa Clara, CA, USA).

Library preparation and sequencing: RNA-seq libraries were prepared using the VAHTS Universal V10 RNA-Seq Library Prep Kit in combination with VAHTS mRNA Capture Beads 2.0 (Vazyme, Nanjing, China), following the manufacturer's instructions (library type: fr-firststrand). Final libraries were quality-checked using the Qubit 3.0 Fluorometer (Invitrogen, Carlsbad, CA, USA) and the Agilent Bioanalyzer DNA assay. Paired-end sequencing (2 × 150 bp) was performed on an Illumina NovaSeq X-Plus platform (Illumina, San Diego, CA, USA).

Bioinformatics analysis: Adaptor sequences and poly(T) tails were trimmed from raw reads using fqtrim (version 0.9.7; http://ccb.jhu.edu/software/fqtrim/). Reads were aligned to the human reference genome (GRCh38) using STAR (v2.7.10a), and gene-level quantification was performed with featureCounts (v2.0.3) using GENCODE v43 annotation. Differential expression analysis was conducted using DESeq2. Genes with a false discovery rate (FDR) < 0.05 were considered significantly differentially expressed. For volcano plot visualization, a more stringent threshold (FDR < 0.0005) and a baseMean > 20 were applied to highlight robust and biologically relevant changes. Specific thresholds used for the volcano plot are detailed in the corresponding figure legend. Gene set enrichment analysis (GSEA) was performed using GSEA software (version 4.4.0, Broad Institute) with predefined gene sets from the Molecular Signatures Database (MSigDB v2024.1). Gene ranking was based on log2 (Fold change) or the ashr shrinkage method implemented in DESeq2. Statistical significance of enrichment was assessed using 10,000 permutations. Gene sets and pathways with FDR < 0.05 were considered significantly enriched. All visualizations were generated using ggplot2 (v3.4.4).

Immunoblot

The cytosolic extracts were obtained using a commercial kit (Active Motif, Carlsbad, CA, USA) following the manufacturer's protocol. For immunoblotting, the following antibodies were used: mouse monoclonal anti-Caspase 3 antibody (Active Motif, Carlsbad, CA, USA) and mouse

monoclonal anti-Vinculin (R&D Systems, Minneapolis, MN, USA) as an internal control. The secondary antibody, peroxidase-conjugated, was anti-mouse (BD Pharmingen, Franklin Lakes, NJ, USA).

Statistical analysis

Data from cell lines are presented as mean ± standard deviation (SD) and were analyzed using one-way ANOVA followed by Tukey's multiple comparisons test. Data from primary cells are shown as median with interquartile range (IQR) and were analyzed using the Friedman test, followed by Dunn's multiple comparisons test, as data were paired. The number of patient samples used for different experiments is specified in each figure legend. Correlation coefficients were calculated using the Spearman rank correlation method. All statistical tests were two-sided, with a significance threshold set at $p < 0.05$. Statistical significance is indicated as follows: $*p < 0.05$, $**p < 0.01$, $***p < 0.001$, $****p < 0.0001$. Data analysis and graphical representations were performed using GraphPad Prism, version 10.1.1 (GraphPad Software Inc., La Jolla, CA, USA).

Supplementary Table

Supplementary Table S1. Main characteristics of MM patients.

PATIENT ID	GENDER	AGE (years)	STAGE	Ig SUBTYPE	LIGHT CHAIN ISOTYPE	% PCs (BMA)	PREVIOUS LINES OF THERAPY*	R-ISS	CYTOGENETIC RISK
MM-1	F	71	ND	IgG	λ	7,5%		I	HR
MM-2	M	57	ND	Light chain	κ	18,0%		I	SR
MM-3	F	82	ND	IgA	κ	19,6%		I	SR
MM-4	F	75	ND	IgA	κ	40,0%		II	SR
MM-5	M	59	ND	IgG	κ	23,0%		I	SR
MM-6	M	57	ND	Light chain	λ	52,0%		III	HR
MM-7	F	66	ND	IgG	λ	53,0%		II	SR
MM-8	F	86	ND	IgG	κ	35,0%		III	HR
MM-9	F	63	ND	Light chain	λ	43,0%		II	SR
MM-10	M	69	ND	IgA	κ	32,0%		II	HR
MM-11	M	73	ND	IgG	κ	34,0%		II	HR
MM-12	M	81	ND	IgA	λ	17,0%		III	HR
MM-13	F	46	ND	IgG	κ	17,0%		I	HR
MM-14	M	58	ND	IgG	λ	42,0%		III	HR
MM-15	F	83	ND	IgG	κ	29,0%		I	SR
MM-16	M	47	ND	IgA	κ	17,0%		I	SR
MM-17	F	85	ND	IgG	κ	23,0%		III	HR
MM-18	M	94	ND	IgG	κ	15,0%		II	SR
MM-19	F	64	ND	IgG	κ	10,0%		II	HR
MM-20	F	82	ND	IgG	λ	13,0%		I	SR
MM-21	F	47	ND	IgA	κ	10,0%		I	HR
MM-22	F	77	ND	Non-secretory		6,0%		II	HR
MM-23	F	48	ND	IgA + BJ	κ	22,0%		III	HR
MM-24	M	67	ND	IgG	κ	24,0%		I	SR
MM-25	M	77	ND	IgG	κ	22,0%		II	HR
MM-26	M	48	ND	IgG	κ	20,0%		II	SR
MM-27	F	48	ND	IgG	κ	30,0%		II	SR
MM-28	F	83	ND	IgA	λ	16,0%		I	HR
MM-29	M	80	RR	IgG	κ	20,4%	2	I	SR
MM-30	M	74	RR	IgA	λ	50,0%	1	III	HR
MM-31	M	77	RR	IgG	λ	20,0%	1	II	SR
MM-32	F	83	RR	IgG	λ	20,0%	1	I	SR
MM-33	F	74	RR	IgG	κ	68,0%	3	III	SR
MM-34	M	79	RR	IgA	κ	10,0%	3	II	SR

MM-35	M	72	RR	IgA	λ	30,0%	3	III	HR
MM-36	M	76	RR	IgG	κ	14,0%	6	II	HR
MM-37	M	64	RR	IgA	κ	40,0%	3	II	HR
MM-38	F	58	RR	IgG	λ	10,0%	1	II	HR
MM-39	M	68	RR	IgA	κ	53,0%	2	III	SR

***** Applicable only to patients with relapsed disease

Abbreviations: MM: multiple myeloma; ND: newly diagnosed; RR: relapsed/refractory; F: female; M: male; Ig: immunoglobulin; BMA: bone marrow aspirate; R-ISS: revised international staging system; HR: high-risk; SR: standard-risk.

SUPPLEMENTARY FIGURES AND FIGURE LEGENDS

Supplementary Figure S1

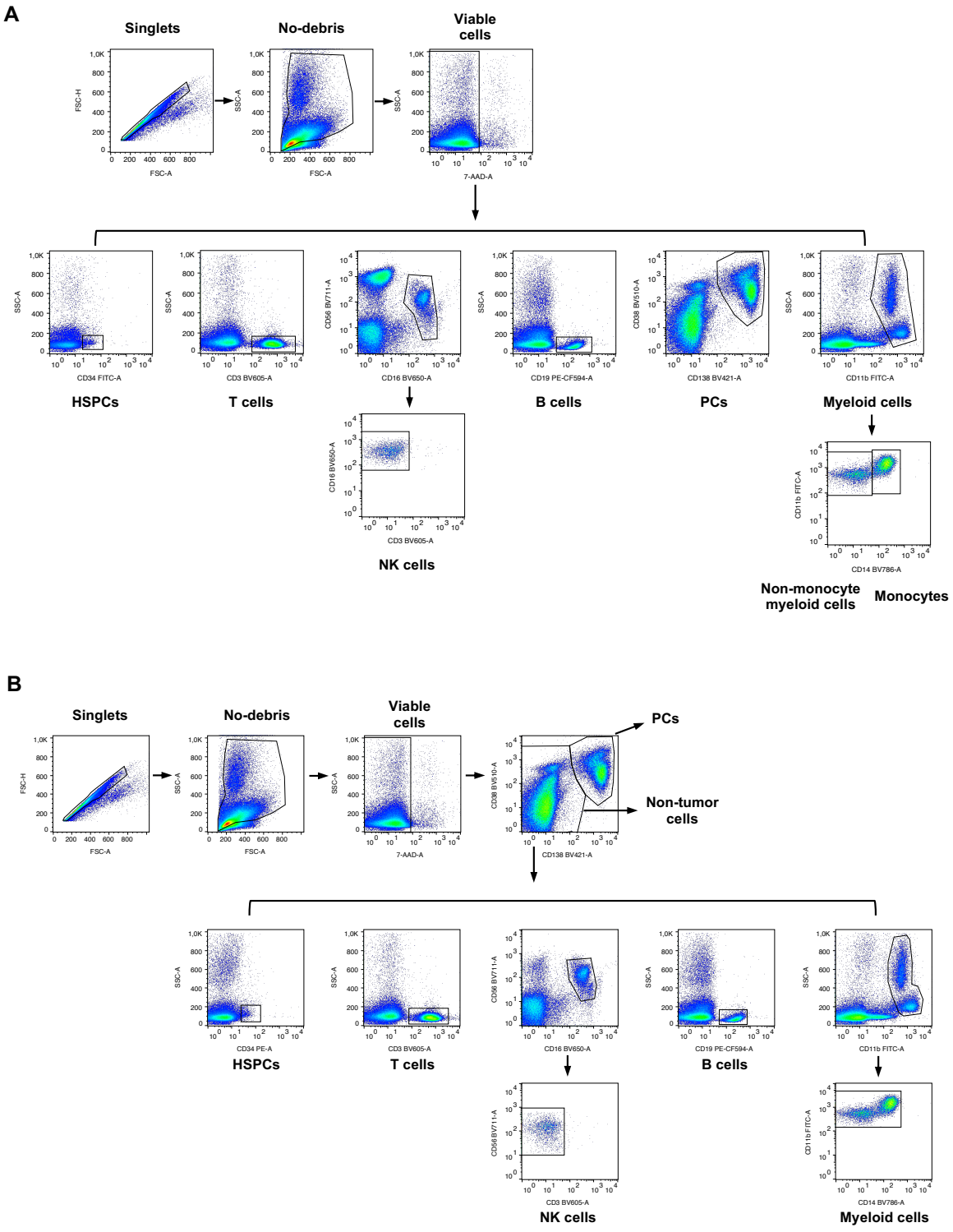

Supplementary Figure S1. Flow cytometry gating strategies for BM subpopulation analysis.

A) Gating strategy for the identification of BM populations in fresh BMMCs stained for CD111 or CD155. Singlets were first gated, followed by the exclusion of debris. Among the no-debris population, viable cells (7-AAD^{-}) were gated. From viable cells, HSPCs (CD34^{+}), T cells (CD3^{+}), NK cells (CD3^{-}CD16^{+}CD56^{+}CD138^{-}), B cells (CD19^{+}), PCs (CD138^{+}CD38^{+}), monocytes (CD11b^{+}CD14$^{dim/+}$), and non-monocyte myeloid cells (SSC^{high}CD11b^{+}CD14^{-}) were identified. PE gates were set using FMO controls. **B)** Gating strategy for BMMC populations after treatment. Singlets were gated, followed by the exclusion of no-debris. Among the no-debris population, viable cells (7-AAD^{-}) were gated. Viable cells were stratified into tumor cells, defined as PCs (CD138^{+}CD38^{+}), and non-tumor cells. Within non-tumor cells, HSPCs (CD34^{+}), T cells (CD3^{+}), NK cells (CD3^{-}CD16^{+}CD56^{+}), B cells (CD19^{+}), and myeloid cells (SSC^{high}CD11b^{+}CD14$^{-/+}$) were identified.

Supplementary Figure S2

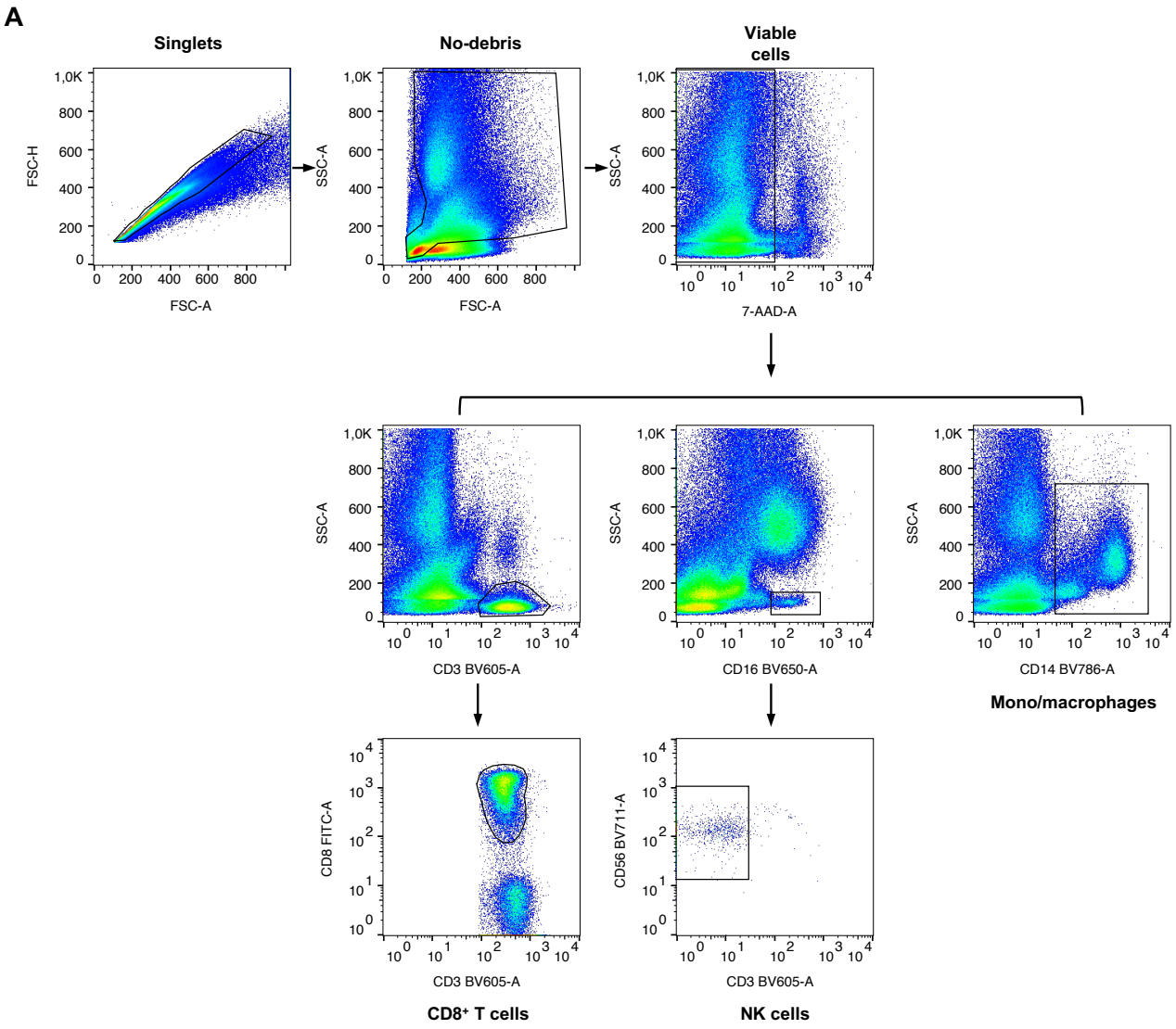

Supplementary Figure S2. Gating strategy for the assessment of CD107a and CD69 expression on BM immune effector cells.

Singlets were first gated, followed by the exclusion of debris. From the no-debris cells, viable cells (7-AAD^-) were gated. Within viable cells, $CD3^+CD8^+$ T cells, NK cells ($CD3^-CD16^+CD56^+CD138^-$), and mono/macrophages ($CD14^{dim/+}$) were identified.

Supplementary Figure S3

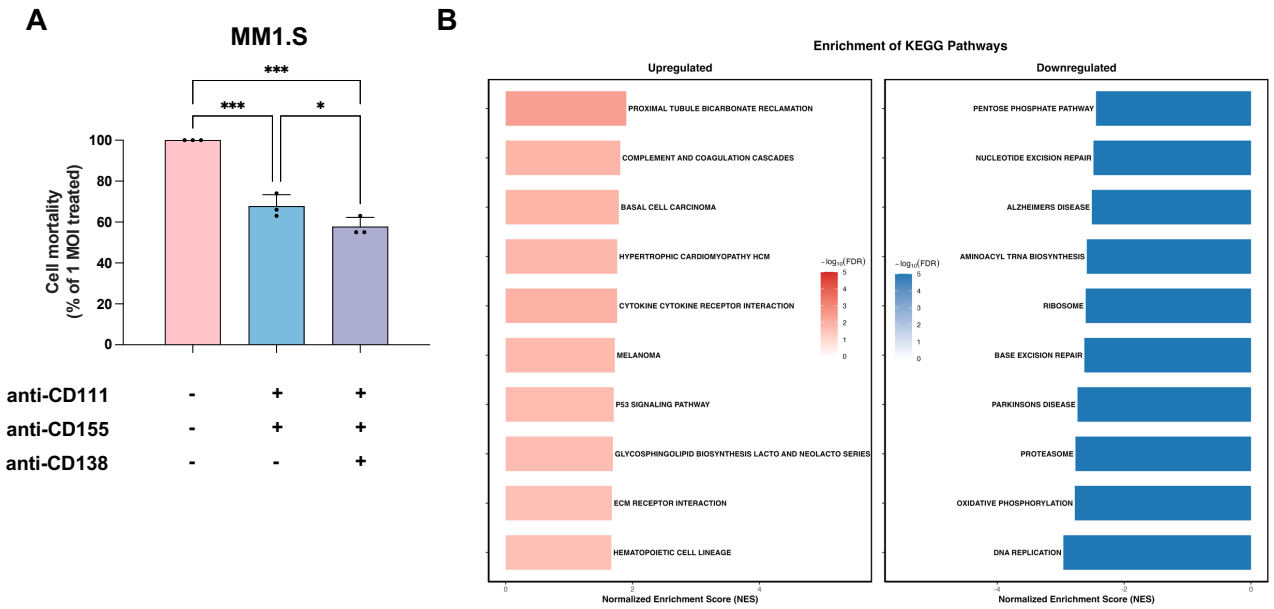

Supplementary Figure S3. BoHV-1 receptor blockade and transcriptional profiling of BoHV-1-infected HMCLs.

A) Relative cell mortality of MM1.S cells pre-treated with CD111, CD155, and CD138 blocking antibodies and infected with BoHV-1 (1 MOI, 48 h), vs infected cells without blockade. Bars indicate mean ± SD; each dot represents an independent experiment (n=3). Statistical analysis was performed using two-way ANOVA with Tukey's multiple comparisons test.

B) KEGG pathway enrichment analysis of JJN-3 cells following BoHV-1 infection (1 MOI, 24 h), showing the top 10 significantly upregulated and downregulated pathways. KEGG pathways were considered significantly enriched at FDR < 0.05. *$p < 0.05$, **$p < 0.01$, ***$p < 0.001$

Supplementary Figure S4

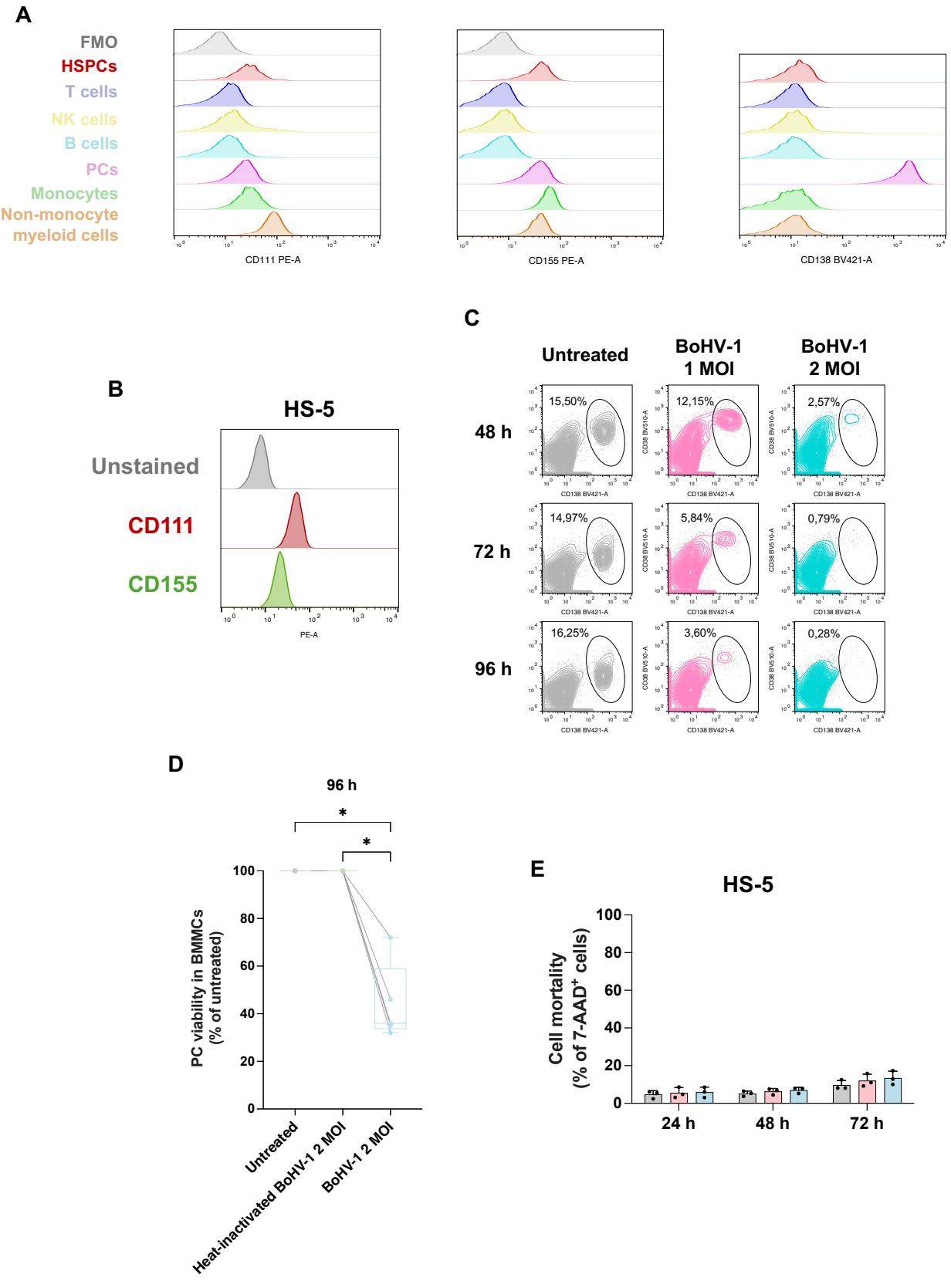

Supplementary Figure S4. BoHV-1 entry receptor expression and cell viability in MM patient cells and HS-5 stromal cells.

A) Flow cytometry histograms from one representative MM patient, showing the expression levels of CD111, CD155, and CD138 on HSPCs, T cells, NK cells, B cells, PCs, monocytes, and non-monocyte myeloid cells. **B)** Flow cytometry histograms showing the CD111 and CD155 expression levels on HS-5 stromal cells. **C)** Representative flow cytometry dot plots showing the percentage of viable PCs within total BMMCs from one MM patient, untreated or BoHV-1-treated (1 and 2 MOI) for 48 h, 72 h, and 96 h. **D)** Relative viability of PCs in total BMMCs from MM patients (n=5) treated with BoHV-1 (heat-inactivated 2 MOI and 2 MOI), for 96 h vs the untreated samples. Each dot represents an individual patient. Bars and boxplots indicate medians with IQR; lines connect paired samples where applicable. **E)** Assessment of cell mortality (as 7-AAD$^+$ cells) in HS-5 stromal cells following BoHV-1 infection at 1 and 2 MOI for 24 h, 48 h, and 72 h.

Each dot represents an independent experiment (n=3); bars indicate mean ± SD. Statistical analyses were performed using the Friedman test with Dunn's multiple comparisons test **(D)** and two-way ANOVA with Tukey's multiple comparisons test (**E)**. *$p < 0.05$

Supplementary Figure S5

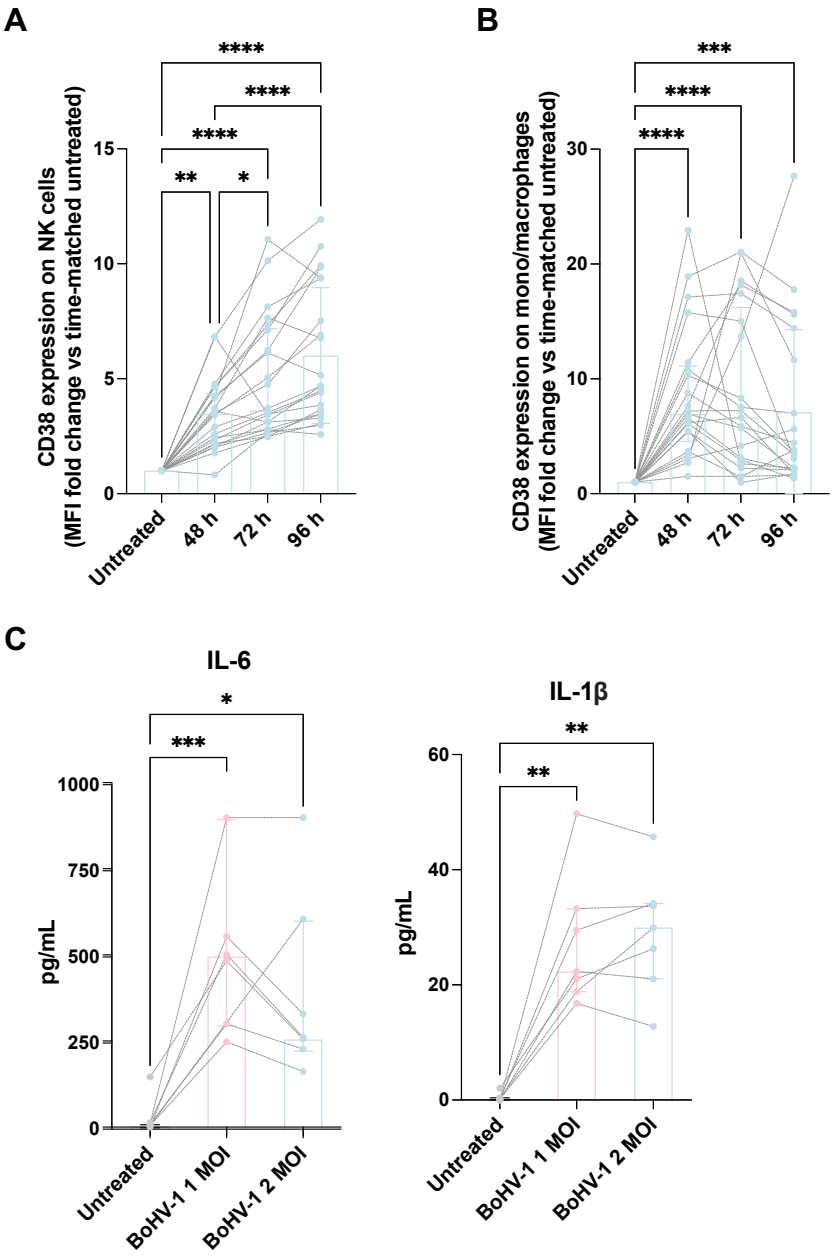

Supplementary Figure S5. Temporal modulation of CD38 expression in NK cells and mono/macrophages and cytokine induction upon BoHV-1 infection.

Relative CD38 expression on **A)** NK cells and on **B)** mono/macrophages among BMMCs treated with BoHV-1 (2 MOI) at 48 h, 72 h, and 96 h compared to time-matched untreated samples (results pooled from 22 patients). **C)** IL-6 and IL-1β levels in the cell-free supernatants of MM patients' BMMCs (n=7) treated with or without BoHV-1 (1 and 2 MOI for 48 h).

Each dot represents an individual patient. Bars and boxplots indicate medians with IQR; lines connect paired samples where applicable. Statistical analyses were performed using the Friedman test with Dunn's multiple comparisons test. *$p < 0.05$, **$p < 0.01$, ***$p < 0.001$, ****$p < 0.0001$

Supplementary Figure S6

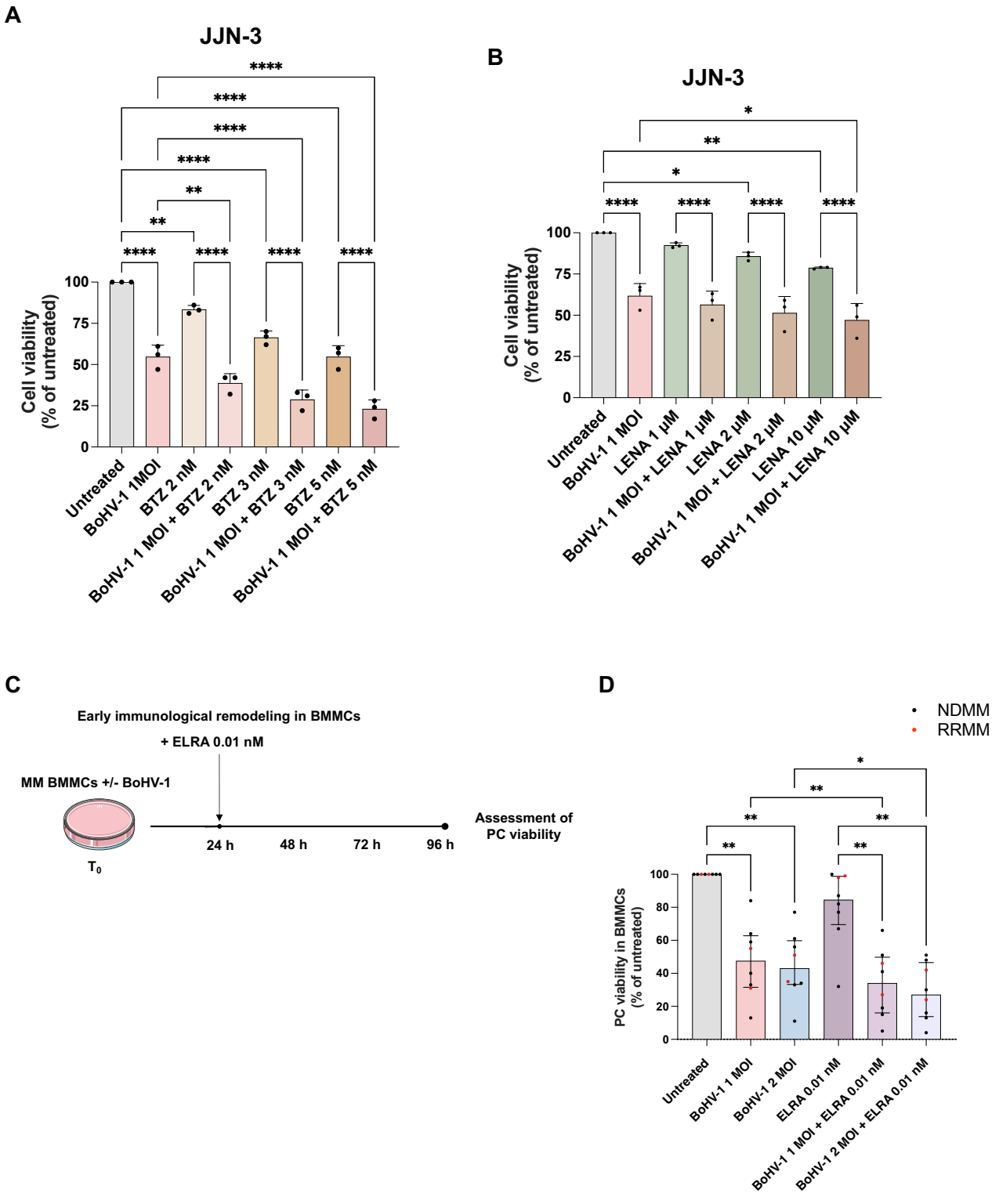

Supplementary Figure S6. Experimental design and functional evaluation of BoHV-1–based combination treatments.

A) Relative viability of JJN-3 cells 72 h after treatment with BoHV-1 (1 MOI), BTZ (2, 3, or 5 nM), alone or in combination. **B**) Relative viability of JJN-3 cells 72 h after treatment with BoHV-1 (1 MOI), LENA (1, 2, or 10 μM), alone or in combination. **C)** Experimental design for BoHV-1 and ELRA combination. **D)** Relative viability of PCs from MM patients' BMMCs 96 h after treatment with BoHV-1 (1 and 2 MOI), ELRA (0.01 nM), alone or in combination (n=8).

Each treatment condition was compared with the untreated control. Data from JJN-3 cells are presented as mean ± SD from three independent experiments. Statistical analysis was performed using repeated-measures one-way ANOVA with Tukey's multiple comparisons test. Data from patient-derived BMMCs are presented as median and IQR from paired experiments. Black dots represent patients with NDMM, while red dots represent those with RRMM. Statistical analysis was performed using the Friedman test with Dunn's correction. *$p < 0.05$, **$p < 0.01$, ****$p < 0.0001$